INTERNATIONAL JOURNAL OF HYDROGEN ENERGY 40 (2015) 9885–9906

Available online at www.sciencedirect.com

ScienceDirect

journal homepage: www.elsevier.com/locate/he

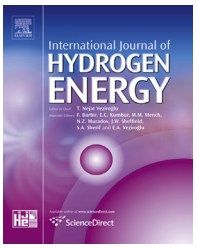

Design of an efficient, high purity hydrogen generation apparatus and method for a sustainable, closed clean energy cycle

Alvin G. Stern *

AG STERN, LLC, Newton, MA, 02467, USA

ARTICLE INFO

Article history:
Received 13 November 2014
Received in revised form
2 May 2015
Accepted 15 May 2015
Available online 9 July 2015

Keywords:
Hydrogen generating apparatus
Hydrogen on demand
Safe hydrogen generation
Hydrogen energy cycle
Sodium metal
Water reactant
Sodium hydroxide byproduct
Clean energy cycle

ABSTRACT

In this paper we present a detailed design study of a novel apparatus for safely generating hydrogen (H_2) on demand according to a novel method, using a controlled chemical reaction between water (H_2O) and sodium (Na) metal that yields hydrogen gas of sufficient purity for direct use in fuel cells without risk of contaminating sensitive catalysts. The apparatus consists of a first pressure vessel filled with liquid H_2O with an overpressure of nitrogen (N_2) gas above the H_2O reactant, and a second pressure vessel that stores solid Na reactant. Hydrogen gas is generated above the solid Na when H_2O reactant is introduced using a regulator that senses when the downstream pressure of H_2 gas above the solid Na reactant has dropped below a threshold value. The sodium hydroxide (NaOH) byproduct of the hydrogen producing reaction, is collected within the apparatus for later reprocessing by electrolysis, to recover the Na reactant.

Introduction

There is a growing need in the modern world to provide a transition to renewable fuels from the present large scale use of nonrenewable carbon based fossil fuels in transportation applications. Hydrogen (H_2) which is stored in near limitless quantity in seawater is the only alternative fuel that is more abundant and environmentally cleaner with the potential of having a lower cost than nonrenewable carbon based fossil fuels, assuming that engineering challenges related to safe implementation and economical extraction of the hydrogen are overcome. In this design study paper, we demonstrate through detailed calculation and analysis means, that a novel apparatus and method for safely generating hydrogen fuel at the time and point of use from ordinary salinated (sea) or desalinated (fresh) water (H_2O) will enable a vehicle range exceeding 300 miles per fueling using direct combustion of the H_2 fuel in appropriately configured internal combustion engines of the Otto or Diesel types, which is comparable to the vehicle ranges presently achieved with gasoline or Diesel fuels, while providing a closed clean energy cycle.

The novel hydrogen generation apparatus design enables hydrogen fuel to be released by controlled means from

* Tel.: +1 617 669 6029; fax: +1 617 527 4331.
E-mail address: inquiries@agstern.com.

http://dx.doi.org/10.1016/j.ijhydene.2015.05.111

Nomenclature

a, b, c, d	adjustable parameters
A, B, C, D	adjustable parameters
u, v, w	adjustable parameters
i, j, k	indices
c_p	isobaric heat capacity, J/K·mol
c_{ps}	specific isobaric heat capacity, J/K·kg
c_{ps}^W	specific isobaric heat capacity, pure (VSMOW) water (H_2O) part, J/K·kg
c_{ps}^S	specific isobaric heat capacity, saline part, J/K·kg
C_{OD}	cylinder outer diameter, cm
C_{ID}	cylinder inner diameter, cm
C_t	cylinder wall thickness, mm
C_h	cylinder height, cm
D_{Na}	sodium rod diameter, cm
E_r°	standard reduction half reaction potential, V
E_o°	standard oxidation half reaction potential, V
E_{ov}°	standard overall reaction potential, V
f	specific Helmholtz energy, J/kg
F_D	base flange diameter, cm
F_t	base flange thickness, cm
g	specific Gibbs energy, J/kg
g^W	specific Gibbs energy, pure (VSMOW) water (H_2O) part, J/kg
g^S	specific Gibbs energy, saline part, J/kg
ΔG	change in Gibbs free energy, kJ
ΔG_f°	standard Gibbs free energy of formation, kJ/mol
ΔH	change in enthalpy, kJ
ΔH_f°	standard enthalpy of formation, kJ/mol
ΔH_c°	standard enthalpy of combustion, kJ/mol
h_{Na}	sodium rod height, cm
I_{CELL}	electrolytic cell current, A
K_{15}	seawater conductivity ratio (PSS-78)
m_C	mass, cylinder, g
m_F	mass, base flange, g
m_{VRF}	mass, valves, regulators, fittings, g
m_P	mass, retainer plate, g
$m_{Cell\text{-}empty}$	mass, single cell empty, g
$m_{40Cell\text{-}empty}$	mass, 40 cells empty, kg
$m_{40Cell\text{-}fueled}$	mass, 40 cells fueled, kg
m_{Na}	sodium mass, g
m_{H_2O}	water mass, g
m_{NaOH}	sodium hydroxide mass, g
M	molar mass, g/mol
n	adjustable coefficient
N	adjustable coefficient
P	absolute pressure, Pa
P_d	atmospheric pressure, decibars
P_l	retainer plate length, cm
P_w	retainer plate width, cm
P_t	retainer plate thickness, cm
P_{AD}	retainer plate aperture diameter, cm
S_A	absolute salinity, g/kg
S_R	reference composition salinity, g/kg
S_P	practical salinity (PSS-78)
S_{NaCl-H_2O}	salinity of NaCl–H_2O solution, % weight
ΔS	change in entropy, J/K
S°	standard entropy, J/K·mol
S_{OD}	metal sleeve outer diameter, cm
S_{ID}	metal sleeve inner diameter, cm
t	temperature exponent
T	absolute temperature, ITS-90, K
t_{90}	celsius temperature, ITS-90, °C
T_f	fusion temperature, K
T_b	vaporization temperature, K
T_{fd}	depression of fusion temperature below that of pure water (H_2O), °C
T_{fs}	fusion temperature of seawater, °C
V_C	cylinder volume, cm^3
V_{C1}	cylinder 1 volume, cm^3
V_{C2}	cylinder 2 volume, cm^3
V_{H_2O}	water volume, cm^3
V_{Na}	sodium rod volume, cm^3
V_{NaOH}	sodium hydroxide volume, cm^3
V_{N_2}	nitrogen volume, cm^3
V_{CELL}	electrolytic cell voltage, V
W	mass fraction
$\alpha, \beta, \varepsilon, \gamma$	adjustable parameters
Δ, θ, Ψ	functions in the nonanalytical terms
φ, λ, σ	adjustable parameters of Gaussian bell shaped terms
∂	partial differential
Δ	difference in a quantity
ρ	density, g/cm^3
ρ_{N_2}	density, nitrogen (N_2), kg/m^3
δ_{N_2}	reduced density, nitrogen (N_2), $(\rho_{N_2}/\rho_{c-N_2})$
τ_{N_2}	inverse reduced temperature, nitrogen (N_2), (T_{c-N_2}/T)
π_S	reduced pressure, saline part, $(P - P_0)/P^*$
ξ_S	reduced salinity, saline part, $(S_A/S^*)^{0.5}$
τ_S	reduced temperature, saline part, $(T - T_0)/T^*$
ρ_{H_2O}	density, pure (VSMOW) water (H_2O), kg/m^3
δ_{H_2O}	reduced density, pure (VSMOW) water (H_2O) part, $(\rho_{H_2O}/\rho_{c-H_2O})$
τ_{H_2O}	inverse reduced temperature, pure (VSMOW) water (H_2O) part, (T_{c-H_2O}/T)
μ	viscosity, cP
$\phi_{N_2}^r$	dimensionless Helmholtz energy, nitrogen (N_2), residual part
ϕ_{H_2O}	dimensionless Helmholtz energy, pure water (H_2O)
$\phi_{H_2O}^o$	dimensionless Helmholtz energy, pure water (H_2O), ideal gas part
$\phi_{H_2O}^r$	dimensionless Helmholtz energy, pure water (H_2O), residual part
o	superscript, ideal gas part
r	superscript, residual part
R	molar gas constant, 8.314510 J/K·mol
M_{N_2}	molar mass, nitrogen (N_2), 0.02801348 kg/mol
R_{N_2}	specific gas constant, nitrogen (N_2), 296.80389 J/K·kg
ρ_{c-N_2}	critical density, nitrogen (N_2), 313.299 kg/m^3
T_{c-N_2}	critical temperature, nitrogen (N_2), 126.192 K
M_{H_2O}	molar mass, pure (VSMOW) water (H_2O), 0.018015268 kg/mol

R_{H_2O}	specific gas constant, pure (VSMOW) water (H_2O), 461.51805 J/K·kg	S^*	reducing salinity, 40.188617 g/kg
ρ_{c-H_2O}	critical density, pure (VSMOW) water (H_2O), 322 kg/m^3	T_0	celsius zero point, ITS-90, 273.15 K
T_{c-H_2O}	critical temperature, pure (VSMOW) water (H_2O), 647.096 K	T_{Eu}	eutectic temperature of NaCl–H_2O solution, −21.2 °C
g^*	reducing specific Gibbs energy, 1 J/kg	T^*	reducing temperature, 40 K
P_0	standard atmospheric pressure, 101 325 Pa	ρ_{SS316}	density, SS316 steel, 7.99 g/cm^3
P^*	reducing pressure, 1×10^8 Pa	ρ_{Al}	density, aluminum, 2.70 g/cm^3
		π	number, pi 3.14

ordinary salinated (sea) or desalinated (fresh) water at the time and point of use according to the chemical reaction shown in Eq. (1).

$$2Na_{(s)} + 2H_2O_{(l)} \rightarrow H_{2(g)} + 2NaOH_{(s)} \quad (1)$$

The apparatus implements Eq. (1) to generate hydrogen fuel according to a novel method, where liquid water ($H_2O_{(l)}$) is made to react with solid sodium ($Na_{(s)}$) metal reactant to produce hydrogen ($H_{2(g)}$) gas and sodium hydroxide ($NaOH_{(s)}$) byproduct. Alternative methods for generating hydrogen gas on demand include using high energy chemical compounds such as the alkali metals lithium (Li) or potassium (K) and group I metal hydrides, namely, lithium hydride (LiH) and sodium hydride (NaH), or borohydride/aluminum hydride compounds such as lithium borohydride ($LiBH_4$), sodium borohydride ($NaBH_4$), aluminum borohydride ($Al(BH_4)_3$), lithium aluminum hydride ($LiAlH_4$) and sodium aluminum hydride ($NaAlH_4$) [1–5]. The elements lithium and potassium, however, have relatively low natural abundances of 0.0017% and 1.5%, respectively in the earth's crust and are difficult to extract in concentrated form, while in sea salt which is much easier to recover than land based lithium and potassium ores, sodium ions (Na^+) comprise a large mass fraction of approximately 30.66% compared with a low mass fraction of approximately 1.13% for K^+ and negligible mass fraction for Li^+ [6]. The aforementioned hydride, borohydride and aluminum hydride compounds of Li and Na are difficult to synthesize or manufacture on a very large scale needed for use in motor vehicle transport applications, and therefore become too costly and uneconomical even if they release more hydrogen per unit weight and/or volume than the Li, Na and K elements by themselves. In addition, $Na_{(s)}$ metal can be stored safely under nitrogen (N_2) gas below 300 °C without reacting to form a nitride or azide, in contrast to $Li_{(s)}$ metal which burns in $N_{2(g)}$ and therefore has to be stored under argon (Ar) gas, the latter being far more expensive [7,8]. Other methods of generating hydrogen on demand utilize storage tanks filled with porous metal sponge or powder comprised of light group 1 and 2 metals and/or transition metal elements, namely, Titanium (Ti) or Nickel (Ni). Transition metal based powders absorb hydrogen gas to form corresponding metal hydride (MH_X) compounds that subsequently release the hydrogen when heat is applied [9–12]. Such direct hydrogen storage methods however, are impractical due to the high cost of suitable transition metals Ti and Ni, and moreover, because an infrastructure is needed to supply hydrogen gas directly in large volume to saturate or replenish the metal sponge within the storage reservoir inside a motor vehicle, a procedure fraught with all of the well known safety risks associated with handling large volumes of elemental hydrogen [13,14].

In contrast to the previously described alternative methods for generating hydrogen fuel, the novel apparatus that implements Eq. (1), utilizes low cost reactants, abundant in nature with a direct means of recovering or recycling the products of the hydrogen generating reaction, while also eliminating the risks inherent with handling elemental hydrogen. Sodium (Na) is abundantly available in seawater in the form of sodium chloride (NaCl), and can be readily recovered from the NaOH byproduct of the reaction in Eq. (1), or from a mixture of NaOH and NaCl, using chemical electrolysis according to Eqs. (2) and (3) [15–17].

$$4Na^+ + 4OH^- \rightarrow 4Na_{(l)} + 2H_2O_{(g)} + O_{2(g)} \quad (2)$$

$$2Na^+ + 2Cl^- \rightarrow 2Na_{(l)} + Cl_{2(g)} \quad (3)$$

Electric power required to implement Eqs. (2) and (3) on a large scale to create a sustainable, closed clean energy cycle, can be obtained from large hydroelectric power plants or from advanced solar power plants of a new type, utilizing highly efficient photovoltaic (PV) devices based on a novel, very high transmittance, back-illuminated silicon-on-sapphire wafer substrate being developed by our company AG STERN, LLC, that allows 93.7 percent of the full air mass (AM) 1.5 solar irradiance spectrum to be transmitted into the silicon device layer [18–21]. The advanced solar power plants might use novel PV device panels arrayed vertically on tower type structures in locations with high levels of solar illumination, thereby allowing up to 30 000 PV panels on such a tower to be spatially arrayed and electrically interconnected on a manageable real estate footprint, instead of the existing paradigm of arraying PV panels facing the sun directly on the ground in area inefficient configurations. Many hundreds of such area efficient solar towers could be constructed to produce peak daylight power on a scale that matches the output of commercial nuclear power stations.

The $Na_{(s)}$ reactant and $NaOH_{(s)}$ byproduct in Eq. (1) are environmentally clean substances because although toxic to humans if ingested, they are not carcinogenic or persistent environmental pollutants. The $Na_{(s)}$ metal when exposed to air reacts quickly with oxygen (O_2) to form hygroscopic sodium oxide (Na_2O) that absorbs water to form NaOH that in turn, reacts with carbon dioxide (CO_2) to form sodium

carbonate (Na_2CO_3) and finally sodium hydrogen carbonate ($NaHCO_3$), the latter known as baking soda, as described in Eqs. (4)–(7).

$$4Na_{(s)} + O_{2(g)} \rightarrow 2Na_2O_{(s)} \quad (4)$$

$$Na_2O_{(s)} + H_2O_{(l)} \rightarrow 2NaOH_{(s)} \quad (5)$$

$$2NaOH_{(s)} + CO_{2(g)} \rightarrow Na_2CO_{3(s)} + H_2O_{(l)} \quad (6)$$

$$Na_2CO_{3(s)} + H_2O_{(l)} + CO_{2(g)} \rightarrow 2NaHCO_{3(aq)} \quad (7)$$

By contrast, nonrenewable hydrocarbon based fossil fuels are known carcinogens and persistent environmental pollutants especially of ground water [22–24]. The Eqs. (4)–(7) entail that chemical spills comprised of sodium metal or sodium hydroxide solution will not create the same deleterious effects on the natural environment as the hydrocarbon fuel counterparts.

Hydrogen generation apparatus characteristics

The novel apparatus for generating hydrogen at the point of use shown in Fig. 1 is comprised of two corrosion resistant stainless steel or nickel alloy cylinders having walls sufficiently thick to withstand internal pressures up to 7000 kPa (1015 psi). The two pressure vessels are adjacently positioned and fixed at the base to a retainer plate.

The apparatus in Fig. 1, functions by filling cylinder 1 with either ordinary salinated (sea) or desalinated (fresh) water through the inlet port at valve 1, followed by pressurization of the cylinder with nitrogen (N_2) gas. Flange 1 covers an access port located at the base of cylinder 1 and is only meant to be removed for maintenance or cleaning of the cylinder. The second cylinder 2 contains a solid mass of $Na_{(s)}$ metal that almost completely fills the cylinder, leaving a relatively small unfilled volume near the tapered top section of the cylinder where $H_{2(g)}$ generated by the chemical reaction in Eq. (1) can exist. The solid $Na_{(s)}$ metal cylindrical rod is loaded into cylinder 2 at the access port covered by flange 2. Cylinder 1 contains a riser tube with an inlet that descends nearly to the bottom of the cylinder and an outlet that is connected to the

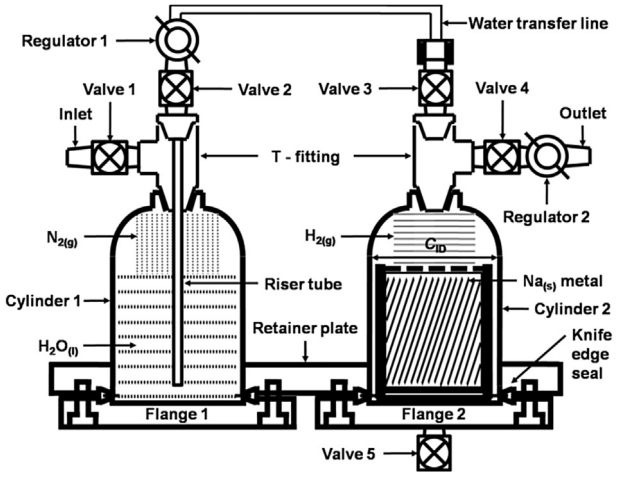

Fig. 1 – Hydrogen generation apparatus.

input port of pressure regulator 1 through valve 2. The riser tube is fixed to cylinder 1 using a bored through compression fitting or a welded connection of the riser tube to an appropriate fitting with a male pipe thread, the latter which is shown in Fig. 1. The pressure regulator 1, senses the downstream pressure of $H_{2(g)}$ above the solid $Na_{(s)}$ metal in cylinder 2, and if the pressure of the $H_{2(g)}$ drops below a threshold value, regulator 1 admits $H_2O_{(l)}$ from cylinder 1 to be transferred into cylinder 2 through valve 3. The $N_{2(g)}$ above the $H_2O_{(l)}$ in cylinder 1 expands to force the $H_2O_{(l)}$ upward through the riser tube and through valve 2, regulator 1 and valve 3, into cylinder 2 where it reacts with the solid $Na_{(s)}$ metal to generate more $H_{2(g)}$ thereby restoring the pressure in cylinder 2 above the $Na_{(s)}$ metal. A second pressure regulator 2, controls the pressure at which $H_{2(g)}$ is delivered downstream from source cylinder 2 through valve 4. For the apparatus to function properly, the downstream $H_{2(g)}$ pressure controlled by regulator 2, must be lower than the $N_{2(g)}$ pressure in cylinder 1 even at the point when all or nearly all of the $H_2O_{(l)}$ in cylinder 1 has been transferred into cylinder 2 by the expanding $N_{2(g)}$. After all of the $Na_{(s)}$ in cylinder 2 has reacted with the $H_2O_{(l)}$ from cylinder 1, a concentrated aqueous solution of $NaOH_{(aq)}$ will have formed in cylinder 2 that must be partially drained out through valve 5, before refueling the apparatus. The collection of the $NaOH_{(aq)}$ from cylinder 2 is essential to ensuring that the $Na_{(s)}$ metal can be recovered according to Eq. (2) to form a sustainable, closed clean energy cycle.

In Table 1, the status of the valves 1–5 in the apparatus is shown during normal operation and also during refueling.

During refueling, the $H_2O_{(l)}$ and $N_{2(g)}$ in cylinder 1 are replenished through the open valve 1 at the inlet port of the apparatus. The concentrated $NaOH_{(aq)}$ solution is partially drained from cylinder 2 through the open valve 5 with the rest being removed as a semisolid when flange 2 is opened, followed by the loading of a fresh $Na_{(s)}$ metal cylindrical rod into cylinder 2. Once refueling has been completed, valves 1 and 5 are closed, and valves 2, 3 and 4 are opened in sequence to commence normal operation.

In an application where the $H_{2(g)}$ fuel is expected to be consumed or burned directly in an Otto type internal combustion engine, the pressure on the process side or output of regulator 2 can be set to a relatively low 200 kPa (29 psi) value, necessitating a pressure on the order of 600 kPa (87 psi) for $H_{2(g)}$ within cylinder 2 on the source side of regulator 2. With careful design, the pressure of the $N_{2(g)}$ in cylinder 1 can be held at or below 3500 kPa (507 psi), thereby maintaining low overall gas pressures in the apparatus for improved safety. Furthermore, by only storing a small volume of the highly flammable and leak prone $H_{2(g)}$ fuel in cylinder 2, catastrophe can be prevented if the integrity of the apparatus becomes compromised and $H_{2(g)}$ leaks occur due to a motor vehicle accident or other circumstances. Actuation of the valves 1–5 shown in Fig. 1, can be manual, pneumatic or

Table 1 – Valve conditions in the apparatus.

	Valve 1	Valve 2	Valve 3	Valve 4	Valve 5
Normal operation	Closed	Open	Open	Open	Closed
Refueling	Open	Closed	Closed	Closed	Open

electropneumatic, however, to reduce the possibility of gas leaks and especially $H_{2(g)}$ leaks in the apparatus, valves 1–5 must be fully sealed, preferably using welded bellows to ensure that the small $H_{2(g)}$ molecules cannot leak around or diffuse through any packing materials. In addition, pipe threads that might normally be sealed using polytetrafluoroethylene (PTFE) compounds, should instead be welded in place to prevent $H_{2(g)}$ leaks.

It is envisioned that the hydrogen generation apparatus will be installed in a mechanically robust, light weight enclosure above the roof or at the rear of an automobile. Placement of the hydrogen generation apparatus in a roof compartment would enable the $H_{2(g)}$ which is significantly lighter than nitrogen and oxygen in air, to readily diffuse upward into the atmosphere in the event of leaks developing, thereby also reducing the risk of any fire that might occur, from spreading into the passenger compartment. Positioning the hydrogen generation apparatus in a rear compartment might be less safe than roof placement, however, it provides easier access to the apparatus for refueling.

Hydrogen generation method

The hydrogen generation apparatus shown in Fig. 1 and described in the section titled Hydrogen generation apparatus characteristics, performs the function of producing hydrogen (H_2) gas according to the chemical reaction given by Eq. (1) that has been known to science since Humphrey Davy first isolated the element sodium (Na) using chemical electrolysis of sodium hydroxide (NaOH) powered by a battery in 1808 [15,25]. The method of generating hydrogen according to Eq. (1) that is implemented by the apparatus shown in Fig. 1, relies on a novel process where instead of adding Na metal in liquid or solid form to a volume of $H_2O_{(l)}$, the $H_2O_{(l)}$ is added to a completely solid mass of $Na_{(s)}$ metal precast into a cylindrical rod shape that fills nearly the entire volume of cylinder 2. It is advantageous not to store or transfer liquid $Na_{(l)}$ metal which has a melting point of 370.95 ± 0.05 K, because $Na_{(l)}$ is much more reactive than solid $Na_{(s)}$ and coupled with a low viscosity of 0.7264 cP at 371.15 K (near the melting point), the liquid $Na_{(l)}$ readily infiltrates packing or sealing materials in pumps and valves, resulting in leaks that can develop into a fire releasing a large amount of heat that can melt the stainless steel containment system [26–30]. The novel method of generating $H_{2(g)}$ according to Eq. (1) therefore eliminates the need for liquefying Na metal or preparing it as a dispersion in an inert carrier liquid to render it transferrable in measured quantity into an $H_2O_{(l)}$ volume [8].

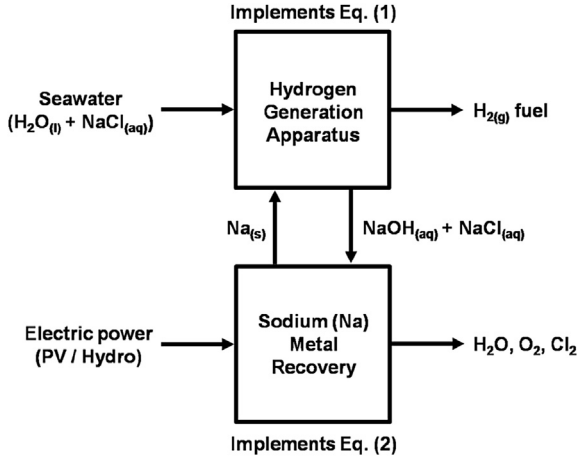

Fig. 2 – Hydrogen fuel, sustainable clean energy cycle diagram.

The complete hydrogen fuel clean energy cycle is illustrated in the diagram in Fig. 2, showing all of the material and energy inputs and outputs of the system.

The novel method further allows the possibility of filling cylinder 1 of the apparatus with seawater directly to react with the solid $Na_{(s)}$ metal in cylinder 2, a unique characteristic of the apparatus which becomes a key factor in enabling the $H_{2(g)}$ generation method to become cost effective for large scale implementation to achieve a sustainable, closed clean fuel cycle for motor vehicle transport applications according to Fig. 2. By filling cylinder 1 shown in Fig. 1 with seawater when the apparatus is refueled as indicated in Fig. 2, additional Na mostly in the form of NaCl is harvested from the sea and becomes mixed or added to the original Na metal that exists in the form of NaOH after reacting with $H_2O_{(l)}$ to generate $H_{2(g)}$ fuel. To calculate how much Na metal can be harvested by fueling cylinder 1 of the hydrogen generation apparatus with seawater as opposed to ordinary freshwater, it is necessary to consider Table 2, that provides the Reference Composition of Standard Seawater (SSW), defined by the Standard Seawater Service to be Atlantic surface seawater collected between 40 and 50° west longitude [6].

As seen in Table 2, the solute in Standard Seawater having the Reference Composition, contains a Na^+ mass fraction given as $W_{Na^+} \approx 0.3066$, that exists primarily in the form of NaCl. Seawater having the Reference Composition shown in Table 2 is known as Reference Seawater. The Reference Composition Salinity S_R provides an estimate of the Absolute

Table 2 – Reference composition of standard seawater at $T = 298.15$ K and $P_0 = 101\,325$ Pa.

	[a]Molar mass (M) [g/mol]	Mass fraction (W)	Ref. seawater ($S_P = 35$) [g/kg]
Na^+	22.98976928(2)	0.3065958	10.78145
Mg^{+2}	24.3050(6)	0.0365055	1.28372
Ca^{+2}	40.078(4)	0.0117186	0.41208
K^+	39.0983(1)	0.0113495	0.39910
Sr^{+2}	87.62(1)	0.0002260	0.00795
Cl^-	35.453(2)	0.5503396	19.35271
SO_4^{2-}	96.0626(50)	0.0771319	2.71235
HCO_3^-	61.01684(96)	0.0029805	0.10481
Br^-	79.904(1)	0.0019134	0.06728
CO_3^{2-}	60.0089(10)	0.0004078	0.01434
$B(OH)_4^-$	78.8404(70)	0.0002259	0.00795
F^-	18.9984032(5)	0.0000369	0.00130
OH^-	17.00733(7)	0.0000038	0.00014
$B(OH)_3$	61.8330(70)	0.0005527	0.01944
CO_2	44.0095(9)	0.0000121	0.00042
Sum		1.0000000	35.16504
H_2O			964.83496
Sum			1000.00000

[a] Molar mass values from Wieser [31].

Salinity for Reference Seawater as well as Standard Seawater and is related to the Practical Salinity S_P according to Eq. (8) [6].

$$S_R = (35.16504/35)\text{g/kg} \times S_P \quad (8)$$

Reference Seawater that has been normalized to a Practical Salinity $S_P = 35$, has a Reference Composition Salinity $S_R = 35.16504$ g/kg as indicated in Table 2. Practical Salinity is a dimensionless quantity defined based on the Practical Salinity Scale (PSS-78) from 1978, using a conductivity ratio K_{15} that represents the electrical conductivity of a seawater sample (at $t_{90} = 14.996$ °C and $P_0 = 101\,325$ Pa) divided by the conductivity of a potassium chloride (KCl) solution at the same temperature and pressure, having a standard concentration of 32.4356×10^{-3} kg of KCl per kg of solution [32,33]. When the ratio $K_{15} = 1$, then the Practical Salinity $S_P = 35$ by definition. If cylinder 1 is filled with Standard Seawater having the Reference Composition shown in Table 2 with a Practical Salinity $S_P = 35$, then the Absolute Salinity will be given by Eq. (8) as $S_R = 35.16504$ g/kg. Thus, every kilogram of the Standard Seawater used to fill cylinder 1 of the apparatus will contain exactly 35.16504 g of sea salt solute that in turn comprises Na primarily in the form of NaCl given as (0.3065958)(35.16504 g) = 10.78145 g of Na per kilogram of Standard Seawater. When the byproducts of the chemical reaction given in Eq. (1) consisting primarily of NaOH and NaCl, the latter obtained from seawater, are recovered and recycled using electrolysis according to Eqs. (2) and (3), more Na metal will have been produced by the electrolysis than was originally available in cylinder 2 when the hydrogen generation apparatus was freshly fueled. Therefore, it becomes possible to passively increase the amount of sodium metal in the closed hydrogen fuel clean energy cycle based on the novel method described that implements Eqs. (1)–(3), without having to invest capital to develop sodium chloride mines or construct large evaporation ponds for seawater to actively recover the sodium chloride from seawater. The very act of refueling the novel apparatus with seawater as indicated in Fig. 2, effectively functions to increase the overall quantity of sodium (Na) in the closed hydrogen fuel clean energy cycle.

Salinity can vary widely in the seas and oceans of the world with the Dead Sea, Red Sea, Persian Gulf and the Mediterranean Sea having the highest salt content while the Baltic Sea, Caspian Sea and Black Sea have the lowest salt content. Therefore, the countries which draw water from the Red Sea, Persian Gulf or the Mediterranean Sea to refuel the hydrogen generation apparatus will collect the largest amount of sodium (Na) from sea salt while countries bordering the Baltic Sea, Caspian Sea and Black Sea might have to send tanker ships to collect seawater from the open expanses of the world's oceans where the salinity is relatively uniform and near in value to the Reference Composition Salinity $S_R = 35.16504$ g/kg corresponding to $S_P = 35$ [34].

Hydrogen generation apparatus design

The novel $H_{2(g)}$ generation method requires a design of the apparatus that allows the chemical reaction described in Eq. (1) to proceed to completion in a form where the solid $Na_{(s)}$ reactant in cylinder 2 is reacted completely with excess $H_2O_{(l)}$ stored in cylinder 1 before the apparatus is refueled. The need to consume the $Na_{(s)}$ reactant fully in cylinder 2 entails utilizing an architecture for the apparatus consisting of at least two cells, with each cell comprising the cylinders 1 and 2 shown in Fig. 1, so that if the $Na_{(s)}$ reactant is consumed in the first cell, the second cell begins generating $H_{2(g)}$ fuel, while the first cell can be refueled, thereby providing uninterrupted delivery of $H_{2(g)}$ to the downstream application such as the internal combustion engine in a vehicle that is being driven on a highway. In practice, it is advantageous to limit the size of cylinder 2 in each cell of the apparatus to avoid storing a single very large mass of reactive and flammable $Na_{(s)}$ metal at one location. A schematic is shown in Fig. 3 of a multicell variant of the apparatus meant to be installed in a motor vehicle.

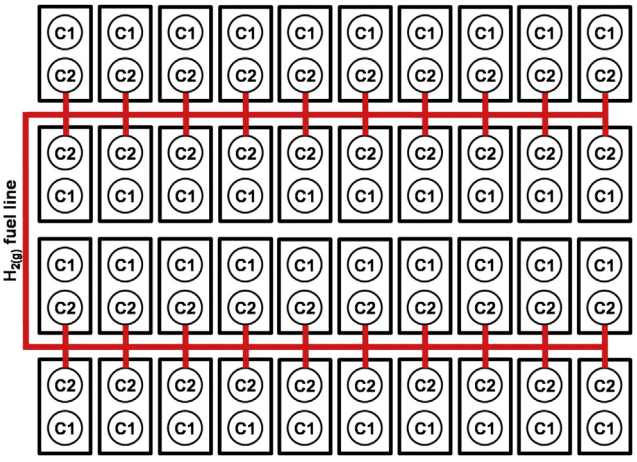

Fig. 3 – Multicell variant of the hydrogen generation apparatus meant to be installed in a motor vehicle.

In Fig. 3, a multicell variant of the hydrogen generation apparatus is shown consisting of 40 cells, with each cell comprising the hardware shown in Fig. 1 including two cylinders indicated as C1 and C2. As the $Na_{(s)}$ reactant is consumed in each of the 40 cells in sequential order, the status of each cell can be provided on a display to apprise the driver of when it is time to refuel the empty cells in the apparatus. To enable the chemical reaction in Eq. (1) to proceed to completion in the hydrogen generation apparatus in a form where the solid $Na_{(s)}$ reactant in cylinder 2 is reacted completely with excess $H_2O_{(l)}$ stored in cylinder 1, the cylinders 1 and 2 in the apparatus must be dimensioned to accommodate the excess $H_2O_{(l)}$ in cylinder 1 needed to react with all of the $Na_{(s)}$ in cylinder 2. Table 3 provides the physical properties of the chemical reactants and products in Eq. (1), needed for calculating an optimum design of the apparatus.

For added safety, it is expedient to limit the internal volume of cylinder 2 to approximately $V_{C2} = 3785$ cm^3 (1 Gal). To facilitate ease of manufacture of the apparatus, cylinder 1 should be identical to cylinder 2, thus $V_{C2} = V_{C1} = V_C$. In Fig. 4, important dimensions of the solid $Na_{(s)}$ metal cylindrical rod and encapsulating sleeve are shown.

In Fig. 4, the solid $Na_{(s)}$ cylindrical rod inside an encapsulating metal sleeve is meant to be loaded as a single unit into

Table 3 – Physical properties of chemical reactants and products in Eq. (1) at $T = 298.15$ K and $P_0 = 101\,325$ Pa.

	Molar mass (M) [g/mol]	Density (ρ) [g/cm^3]
Sodium (Na)	22.989 769 28(2) [31]	0.96601 (31.3 °C) [38]
[a]Pure (VSMOW) Water (H_2O)	18.015 268 [35–37]	0.999 974 95 (3.983 035 °C) [39]
Standard Seawater (SSW, $S_P = 35$)		1.0237 [40]
Hydrogen (H_2)	2.015 88 [31]	0.0823 [41]
Sodium Hydroxide (NaOH)	39.997 109 28 [31]	2.13 [42]

[a] Vienna Standard Mean Ocean Water (VSMOW) [35].

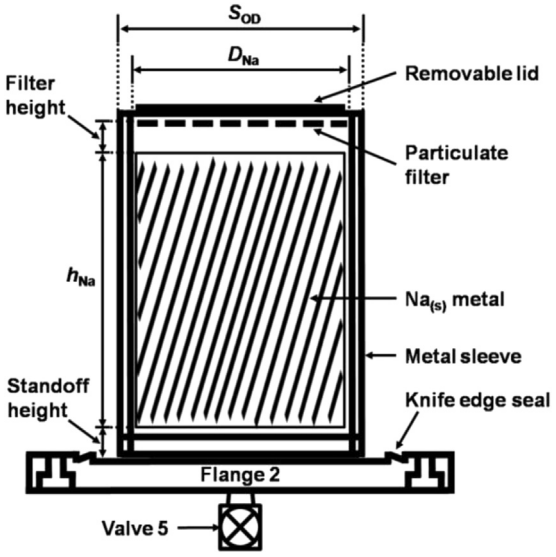

Fig. 4 – Metal sleeve with a removable lid hermetically encapsulates a solid $Na_{(s)}$ metal cylindrical rod.

cylinder 2 which has an internal diameter $C_{ID} = 9.1$ cm as seen in Fig. 1, and is capped at the base by flange 2 using a knife edge seal. In Fig. 4, the solid $Na_{(s)}$ metal cylindrical rod is shown inside the protective metal sleeve, prior to loading into cylinder 2 together with the metal sleeve and flange 2 as one unit. The metal sleeve shown in cross section in Fig. 4, is welded to the interior face of flange 2 and serves the important function of allowing the solid $Na_{(s)}$ cylindrical rod to be packaged or encased hermetically during storage prior to its use, much as a sardine can which can be opened by peeling away a thin, sheet metal lid to open the hermetically sealed container. The metal sleeve in Fig. 4 has an outer diameter $S_{OD} = 8.8$ cm and is meant to be loaded into cylinder 2 as a single unit together with the $Na_{(s)}$ rod during refueling of the hydrogen generation apparatus, after peeling away the removable metal lid that exposes the top of the $Na_{(s)}$ rod to allow it to chemically react with $H_2O_{(l)}$ from cylinder 1. The difference in dimension between the inner diameter of cylinder 2 and the outer diameter of the metal sleeve given as $C_{ID} - S_{OD} = 0.3$ cm, provides ample clearance to allow $H_2O_{(l)}$ introduced from cylinder 1, to percolate to the bottom of cylinder 2 to fill the space between the metal sleeve and inner wall of cylinder 2, thereby precluding any $H_{2(g)}$ from leaking out at the knife edge seal located at the base of cylinder 2. The $H_2O_{(l)}$ can only contact the solid $Na_{(s)}$ rod, at the top of the metal sleeve where the removable lid has been peeled away. The metal sleeve has a wall thickness of 1.5 mm and the solid $Na_{(s)}$ cylindrical rod completely fills it. A particulate filter in Fig. 4 made of a metal mesh is integrated into the metal sleeve above the solid $Na_{(s)}$ cylindrical rod to prevent NaOH debris from becoming airborne inside cylinder 2, while still allowing the $H_2O_{(l)}$ reactant to flow to the $Na_{(s)}$ metal and react with it to generate $H_{2(g)}$ fuel. A second filter constructed into regulator 2, uses a small disk of palladium (Pd) to filter out any water molecules mixed with the $H_{2(g)}$, thus allowing only the $H_{2(g)}$ to diffuse through the solid palladium to enter regulator 2 and be delivered to the downstream application. The diameter of the solid $Na_{(s)}$ rod is given as $D_{Na} = 8.5$ cm with a height $h_{Na} = 55$ cm, yielding a volume of $V_{Na} = \pi(D_{Na}/2)^2 h_{Na} = 3119.4$ cm^3. Using the values in Table 3, the mass of the $Na_{(s)}$ metal is calculated as $m_{Na} = \rho V_{Na} = (0.96601\ \text{g/cm}^3)(3119.4\ \text{cm}^3) = 3013.4$ g. The corresponding number of moles of $Na_{(s)}$ metal can be calculated to yield 3013.4 g/22.989 g/mol = 131.1 mol. According to the chemical reaction in Eq. (1), consuming 131.1 mol of $Na_{(s)}$ would necessitate reacting with an equal number of moles of $H_2O_{(l)}$ that corresponds to a mass given as $m_{H_2O} = (18.015\ \text{g/mol})(131.1\ \text{mol}) = 2361.8$ g. Assuming that cylinder 1 is filled with pure (VSMOW) $H_2O_{(l)}$ the volume occupied is calculated to be $V_{H_2O} = m_{H_2O}/\rho = 2361.8\ \text{g}/0.99997495\ \text{g/cm}^3 = 2361.9\ \text{cm}^3$. If cylinder 1 has the same size and dimensions as cylinder 2, with an identical internal volume of $V_{C1} = 3785$ cm^3 (1 Gal), then the unfilled volume in cylinder 1 will be $3785\ \text{cm}^3 - 2361.9\ \text{cm}^3 = 1423.1\ \text{cm}^3$. After all 131.1 mol of $Na_{(s)}$ have reacted in cylinder 2 according to Eq. (1), 131.1 mol of NaOH will have formed, corresponding to a mass $m_{NaOH} = (39.997\ \text{g/mol})(131.1\ \text{mol}) = 5243.6$ g. The volume occupied by 5243.6 g of NaOH is calculated to be $V_{NaOH} = m_{NaOH}/\rho = 5243.6\ \text{g}/2.13\ \text{g/cm}^3 = 2461.8\ \text{cm}^3$.

A compromise in the design is needed to determine how the unfilled volume of 1423.1 cm^3 in cylinder 1 will be allocated between excess $H_2O_{(l)}$ needed to produce a concentrated aqueous $NaOH_{(aq)}$ solution in cylinder 2 versus $N_{2(g)}$ gas pressure needed to transfer the $H_2O_{(l)}$ from cylinder 1 into cylinder 2. To determine how much excess $H_2O_{(l)}$ should be added to cylinder 1 beyond the calculated $m_{H_2O} = 2361.8$ g needed for a stoichiometric reaction with $Na_{(s)}$ in cylinder 2, the melting point of the concentrated aqueous $NaOH_{(aq)}$ solution must be considered since it would be ideal to be able to drain it from cylinder 2 through valve 5 during refueling of the hydrogen generation apparatus.

Sodium hydroxide ($NaOH_{(s)}$) is infinitely miscible with water $H_2O_{(l)}$ however, the eutectic mixture of an NaOH–H_2O binary solution occurs at approximately 18.5% weight NaOH with 81.5% weight H_2O and corresponds to a freezing point of −29 °C [43–45]. Although it would be ideal to form a eutectic

18.5% weight NaOH in H_2O solution in cylinder 2 after all of the $H_2O_{(l)}$ from cylinder 1 has been transferred, for an NaOH mass of 5243.6 g, a eutectic solution would necessitate an $H_2O_{(l)}$ mass transfer of 23 100.2 g from cylinder 1 to cylinder 2. Such a large quantity of $H_2O_{(l)}$ would require an increase in volume of the cylinders 1 and 2 at least six times greater than the present design volumes of 3785 cm^3 (1 Gal), making the cost of the hydrogen generation apparatus prohibitive and also wasteful in terms of space, since only a relatively small fraction of the volume in cylinder 2 would be utilized for $Na_{(s)}$ metal storage. Instead, a more practical solution would allocate 2500 cm^3 out of the 3785 cm^3 internal volume of cylinder 1 for $H_2O_{(l)}$, thereby providing an excess volume of $H_2O_{(l)}$ beyond the stoichiometric quantity, calculated to be 2500 cm^3 − 2361.9 cm^3 = 138.1 cm^3 or m_{H_2O} = (2500 cm^3)(0.99997495 g/cm^3) = 2499.9 g, to ensure that all of the $Na_{(s)}$ metal in cylinder 2 reacts to liberate $H_{2(g)}$ according to Eq. (1).

The absence of a eutectic 18.5% weight NaOH in H_2O solution in cylinder 2 after all of the $Na_{(s)}$ metal has reacted according to Eq. (1), entails that during refueling of the apparatus, most of the highly concentrated aqueous $NaOH_{(aq)}$ solution cannot be directly drained out to a storage tank prior to removing flange 2 with attached metal sleeve shown in Fig. 4, because the NaOH at or near room temperature exists as a solid. Applying external heat to cylinder 2 to liquefy the NaOH is not practical due to the added complexity of installing heaters. Thus, valve 5 is opened to drain away from cylinder 2 any of the excess $H_2O_{(l)}$ that remains in a liquid state, before removing flange 2 with the attached metal sleeve that formerly contained the solid $Na_{(s)}$ rod and now contains the solid NaOH byproduct of the chemical reaction shown in Eq. (1). After the NaOH byproduct is removed from cylinder 2, it can be stored under $N_{2(g)}$ blanketing gas until it is ready to be reprocessed according to Eq. (2) to recover the $Na_{(s)}$ metal.

The volume available in cylinder 1 for $N_{2(g)}$ needed for transferring the $H_2O_{(l)}$ out of cylinder 1 and into cylinder 2 is calculated to be V_{N_2} = 3785 cm^3 − 2500 cm^3 = 1285 cm^3.

The mass of the hydrogen generation apparatus shown in Fig. 3, consisting of 40 cells can be calculated by assuming that all its major components including cylinders 1 and 2 with base flanges 1 and 2, valves, regulators and fittings are constructed using grade 316 stainless steel with density ρ_{SS316} = 7.99 g/cm^3, offering enhanced corrosion resistance to seawater [46]. The inner diameter of cylinder 2 is given as C_{ID} = 9.1 cm as seen in Fig. 1 and assuming a cylinder wall thickness C_t = 1.6 mm (0.063″) considered sufficiently thick to withstand internal pressures up to 7000 kPa (1015 psi), the cylinder outer diameter is given as C_{OD} = 9.42 cm. Taking a cylinder height C_h = 58.2 cm, the mass of the grade 316 stainless steel cylinder can be estimated as $m_C = [\pi C_h\{(C_{OD}/2)^2 - (C_{ID}/2)^2\}] \times \rho_{SS316}$ = 2164.5 g. Base flanges 1 and 2 each have a diameter F_D = 15 cm and thickness F_t = 0.32 cm, and therefore a mass calculated as $m_F = [\pi F_t(F_D/2)^2] \times \rho_{SS316}$ = 451.8 g. The retainer plate is rectangular in shape with length P_l = 25 cm, width P_w = 15 cm and thickness P_t = 0.95 cm, with two circular apertures of diameter P_{AD} = 9.5 cm for installing cylinders 1 and 2. The retainer plate is not in direct contact with any of the chemical reactants and products in Eq. (1), and therefore can be fabricated from light weight aluminum with density ρ_{Al} = 2.70 g/cm^3 [46]. The mass of the retainer plate is calculated as $m_P = [(P_l \times P_w \times P_t) - 2\pi P_t(P_{AD}/2)^2] \times \rho_{Al}$ = 603.6 g. The weight of the valves 1–4, regulators 1 and 2 and fittings add approximately m_{VRF} = 2000 g (4.4 lbs) more to the overall mass of each cell of the hydrogen generation apparatus. The unfueled mass of a single cell of the hydrogen generation apparatus shown in Fig. 1 is therefore calculated as $m_{Cell\text{-}empty} = 2m_C + 2m_F + m_P + m_{VRF}$ = 7836.2 g (17.3 lbs). Thus, the unfueled mass of the hydrogen generation apparatus with 40 cells as seen in Fig. 3, becomes $m_{40Cell\text{-}empty} = 40 \times m_{Cell\text{-}empty}$ = 313.4 kg and fully fueled, will have a mass of approximately $m_{40Cell\text{-}fueled} = m_{40Cell\text{-}empty} + 40(m_{Na} + m_{H2O})$ = 533.9 kg. Use of composite material for the cylinders would lighten the apparatus considerably. Table 4 summarizes important design parameter values for the hydrogen generation apparatus.

Hydrogen generation apparatus operating characteristics

For the novel hydrogen generation method according to Eq. (1) to be viable for use in motor vehicle transport applications, the apparatus described in detail in the section titled Hydrogen generation apparatus design, must be capable of functioning under a wide range of ambient temperatures, from the extreme cold prevalent at the South Pole to the extreme heat of the Mojave and other deserts. The requirement for the apparatus to function reliably under the most extreme temperatures entails first, that the reactants and products in Eq. (1) do not undergo phase transitions between solid, liquid or gas states due to the ambient temperature and also, that the thermodynamics of the chemical reaction described in Eq. (1) remain stable over the full range of temperatures to allow the forward reaction to proceed to completion. Table 5 lists the freezing and boiling points for the reactants and products in Eq. (1) as well as for 2,2,4-Trimethylpentane (C_8H_{18}) or Isooctane, more colloquially known as 100 octane gasoline, and

Table 4 – Design parameters of the hydrogen generation apparatus.

	Outer diameter [cm]	Inner diameter [cm]	Height [cm]	Volume [cm^3]	Mass [kg]	Chemical quantity [mol]
Cylinders 1 and 2	9.42	9.1	58.2	3785	2.1645	
Metal sleeve	8.8	8.5	56	3176.1		
Sodium ($Na_{(s)}$)	8.5		55	3119.4	3.0134	131.1
Pure (VSMOW) $H_2O_{(l)}$				2500	2.4999	138.8
Sodium hydroxide (NaOH)				2461.8	5.2436	131.1
Nitrogen ($N_{2(g)}$)				1285		
Hydrogen generator (40 cells), empty					313.4	
Hydrogen generator (40 cells), fueled					533.9	

Table 5 – Fusion and vaporization temperatures at $P_0 = 101\,325$ Pa.

	Fusion temperature (T_f) [K]	Vaporization temperature (T_b) [K]
Sodium (Na)	370.95 ± 0.05 [26]	1154.5 ± 4.7 [53]
[a]Pure (VSMOW) Water (H_2O)	273.152518 ± 0.000002 [47,48]	373.124 [35]
Hydrogen (H_2)	13.95 [49]	20.4 [54]
Sodium Hydroxide (NaOH)	594 ± 2 [50]	1661.15 [55]
2,2,4-Trimethylpentane (C_8H_{18})	165.785 ± 0.013 [51]	371.35 [56,57]
n-Dodecane (n-$C_{12}H_{26}$) (Diesel No. 1)	263.589 [52]	489.35 [56,57]

[a] Air free water as opposed to air-saturated water, the latter having a freezing point $T = 273.1501$ K [58].

diesel No. 1 or kerosene, represented by n-Dodecane (n-$C_{12}H_{26}$), for comparison.

The freezing and boiling point values listed in Table 5, can be understood in a clearer context when considering that the lowest surface air temperature ever recorded on earth was −89.2 °C at the South Pole, while the highest ever surface air temperature of 56.7 °C was recorded on July 10, 1913 in Death Valley in the Mojave desert California, corresponding to $T = -89.2\ ^\circ\text{C} + T_0 = 183.95$ K and $T = 56.7\ ^\circ\text{C} + T_0 = 329.85$ K, respectively, where $T_0 = 273.15$ K is defined as equal to 0 °C according to the ITS-90 temperature scale [59–62]. The novel hydrogen generation apparatus must therefore be capable of functioning over the relatively wide range of terrestrial temperatures.

As shown in Table 5, the 2,2,4-Trimethylpentane or 100 octane gasoline fuel does not undergo phase transitions over the temperature range from −89.2 °C (183.95 K) to 56.7 °C (329.85 K), rendering it ideal for use even in the most extreme terrestrial environments. Diesel No. 1 or kerosene however, requires special additives to prevent the phase transition to a solid under South Pole type weather conditions. Sodium (Na) metal exists as a solid over the full temperature range (183.95 K–329.85 K) and does not undergo any phase transitions between the solid, liquid and vapor states. Pure (VSMOW) water (H_2O) however, undergoes a transition from the liquid to the solid state at the fusion temperature $T_f \approx 273.15$ K. The transition of pure (VSMOW) liquid water ($H_2O_{(l)}$) to a solid presents a challenge for operating the hydrogen generation apparatus in winter weather conditions that are prevalent for many months of the year at higher, nontropical latitudes, since pure (VSMOW) water ($H_2O_{(l)}$) in cylinder 1 cannot be transferred into cylinder 2 to react with solid $Na_{(s)}$ to produce $H_{2(g)}$ if the ambient temperature drops below $T_f \approx 273.15$ K. A remedy to the high freezing point problem of pure (VSMOW) $H_2O_{(l)}$ can be implemented by adding sodium chloride (NaCl) as a solute to pure (VSMOW) $H_2O_{(l)}$ to lower the freezing point of the aqueous solution reactant used to fill cylinder 1 in the hydrogen generation apparatus. The freezing point depression of $H_2O_{(l)}$ as a function of the dissolved NaCl solute concentration can be calculated according to Eq. (9) [63,64].

$$S_{NaCl-H_2O} = 0.00 + 1.78T_{fd} - 0.0442T_{fd}^{\ 2} + 0.000557T_{fd}^{\ 3} \quad (9)$$

In Eq. (9), S_{NaCl-H_2O} represents the salinity as a weight percentage of NaCl in NaCl–H_2O solution and T_{fd} represents the depression of the freezing point below that of pure water in degrees Celsius. By dissolving sodium chloride in pure water, it becomes possible to lower the freezing point of the aqueous solution down to the eutectic point for NaCl–H_2O solution which is given as $T_{Eu} = -21.2$ °C as seen in Fig. 5.

In Fig. 5, the eutectic temperature of the aqueous NaCl–H_2O solution $T_{Eu} = -21.2$ °C is reached for a salinity value $S_{NaCl-H_2O} = 23.18\%$. For most fueling applications in the United States of America (U.S.A.), a eutectic mixture of NaCl–H_2O will be adequate for use during the winter season to prevent the aqueous solution in cylinder 1 from freezing since temperatures in the conterminous 48 states rarely fall below −20 °C, with the exception of the northern most regions of Minnesota and North Dakota [65]. If the hydrogen generation apparatus is operated at temperatures of −89.2 °C (183.95 K) at the South Pole, below the eutectic temperature ($T_{Eu} = -21.2$ °C) of the aqueous NaCl–H_2O solution, for example, to supply electric power free of carbon emissions for environmental monitoring equipment, then it would become necessary to provide external heating to cylinder 1 to maintain the eutectic brine content in a liquid state.

In large scale operation of the hydrogen generation apparatus for motor vehicle transport applications, sodium chloride (NaCl) would not be added directly as a solute to lower the freezing point of pure (VSMOW) $H_2O_{(l)}$ used to fill cylinder 1, due to the existence of a more cost effective alternative, namely, seawater. Standard Seawater at the Reference Composition and Practical Salinity $S_P = 35$ shown in Table 2, already contains 10.78145 g of Na (mostly as NaCl) per kilogram, that can be further concentrated by evaporating some of the $H_2O_{(l)}$ to yield an aqueous brine solution having a weight percent salinity value contributed only by the NaCl portion of the solute of $S_{NaCl-H_2O} = 23.18\%$, corresponding to the eutectic temperature $T_{Eu} = -21.2$ °C established for NaCl–H_2O solution shown in Fig. 5. The Standard Seawater thus concentrated by

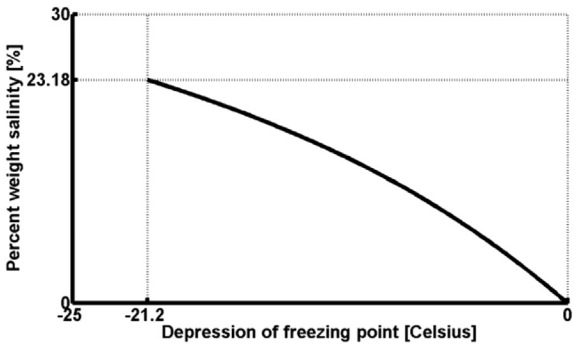

Fig. 5 – Salinity of NaCl–H_2O solution as a function of the freezing point depression.

evaporation can be stored during warm summer months and used for fueling cylinder 1 of the hydrogen generation apparatus during winter months when ordinary Standard Seawater with Practical Salinity $S_P = 35$ might freeze. The fusion temperature lowering of seawater as a function of the salinity is described by Eq. (10) [66].

$$T_{fs} = -0.0575\,S_P + (1.710523\times10^{-3})\,S_P^{3/2} - (2.154996\times10^{-4})\,S_P^{2} - (7.53\times10^{-4})\,P_d \quad (10)$$

In Eq. (10), T_{fs} represents the fusion temperature of seawater in degrees Celsius, P_d represents the atmospheric pressure in decibars, and S_P represents the dimensionless practical salinity defined in the section titled Hydrogen generation method. Eq. (10) is considered to be valid for $4 < S_P < 40$, and is shown plotted in Fig. 6 as a solid line over the stated validity range, however, the fusion temperature values for $S_P > 40$ can be extrapolated using Eq. (10) as represented by the dashed line in Fig. 6.

In Fig. 6, Eq. (10) is plotted up to a Practical Salinity $S_P = 251$, well beyond the specified validity range of the equation, to yield the fusion temperature of the seawater $T_{fs} = -21.2$ °C, that is equivalent to the eutectic temperature of a 23.18% by weight NaCl in NaCl–H_2O solution shown in Fig. 5. If the seawater is further assumed to have the Reference Composition described in the section titled Hydrogen generation method, then Eq. (8) can be used to convert the Practical Salinity value $S_P = 251$ to an absolute salinity value, yielding $S_R = (35.16504/35)\text{g/kg} \times S_P = (35.16504/35) \times 251 = 252.18$ g of sea salt solute per kilogram of seawater solution. Such a high concentration of sea salt solute in seawater having the Reference Composition described in Table 2, corresponds to a 25.2% by weight sea salt solute in Reference Composition Seawater, which matches very closely with the empirical value of 23.18% by weight NaCl in NaCl–H_2O solution shown in Fig. 5 as might be expected. Thus, using a concentrated brine solution formed by evaporating seawater harvested directly from the ocean where it is abundantly available, to fill cylinder 1 of the hydrogen generation apparatus during winter months, can become a cost effective and workable solution to the phase transition problem of the water reactant in Eq. (1).

After fueling cylinder 1 with seawater that has been allowed to evaporate into a concentrated brine solution as described above, with a fusion temperature $T_f \approx 251.95$ K (−21.2 °C), the cylinder has to be pressurized using $N_{2(g)}$ that can expand to force the liquid seawater ($H_2O_{(l)}$) upward through the riser tube shown in Fig. 1 and into cylinder 2, where it can react with $Na_{(s)}$ to generate $H_{2(g)}$ fuel according to Eq. (1). The worst case scenario that must be considered during operation of the hydrogen generation apparatus, assumes that cylinder 1 is pressurized with $N_{2(g)}$ when the ambient air temperature is at a maximum of 56.7 °C (329.85 K), yet, the $N_{2(g)}$ gas expansion that transfers the concentrated aqueous brine solution from cylinder 1 into cylinder 2, occurs when the ambient air temperature has dropped to −21.2 °C (251.95 K). Although such a scenario appears implausible, it could in fact correspond to reality since fueling of the hydrogen generation apparatus in a very cold climate might occur inside a heated edifice rather than outdoors. The final $N_{2(g)}$ pressure in cylinder 1 can be calculated after it has expanded from an initial volume $V_{N_2} = 1285$ cm^3 to a final volume $V_{C1} = 3785$ cm^3, the latter representing the volume of cylinder 1, as a function of the initial pressure of the $N_{2(g)}$ in cylinder 1 which depends on the temperature, by using Eq. (11) derived from the equation of state for nitrogen given in terms of the specific Helmholtz energy [67].

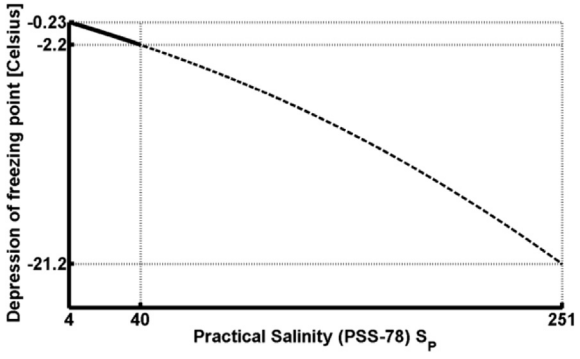

Fig. 6 – Freezing point lowering of seawater as a function of the Practical Salinity (PSS-78) using broad extrapolation.

$$P = \rho_{N_2} R_{N_2} T\left[1 + \delta_{N_2}\left(\partial\phi^r_{N_2}\Big/\partial\delta_{N_2}\right)_{\tau_{N_2}}\right] \quad (11)$$

$$\delta_{N_2}\left(\frac{\partial\phi^r_{N_2}}{\partial\delta_{N_2}}\right)_{\tau_{N_2}} = \sum_{i=1}^{6} u_i N_i \delta_{N_2}^{u_i}\tau_{N_2}^{v_i} + \sum_{i=7}^{32} N_i \delta_{N_2}^{u_i}\tau_{N_2}^{v_i} exp\left(-\delta_{N_2}^{w_i}\right) \times \left(u_i - w_i\delta_{N_2}^{w_i}\right) + \sum_{i=33}^{36} N_i \delta_{N_2}^{u_i}\tau_{N_2}^{v_i} exp\left(-\varphi_i(\delta_{N_2}-1)^2 - \lambda_i(\tau_{N_2}-\sigma_i)^2\right)\left[u_i - 2\delta_{N_2}\varphi_i(\delta_{N_2}-1)\right]$$

The coefficients and parameters required for calculating Eq. (11) for the final $N_{2(g)}$ pressure in cylinder 1 of the hydrogen generation apparatus are provided in Table A.1 in Appendix A. In Eq. (11), the absolute pressure P is given in pascals (Pa), the absolute temperature T is given in Kelvin (K), the density ρ_{N_2} is given in kg/m^3, the reduced density $\delta_{N_2} = \rho_{N_2}/\rho_{c-N_2}$, the inverse reduced temperature $\tau_{N_2} = T_{c-N_2}/T$, and the specific gas constant is defined as $R_{N_2} = R/M_{N_2}$, where the molar gas constant $R = 8.314510$ J/K·mol and the molar mass $M_{N_2} = 0.02801348$ kg/mol for nitrogen (N_2). The critical temperature $T_{c-N_2} = 126.192$ K, and the critical density $\rho_{c-N_2} = 313.299$ kg/m^3 for N_2. If cylinder 1 of the hydrogen generation apparatus is pressurized with $N_{2(g)}$ at a temperature $T = 329.85$ K (56.7 °C), then Eq. (11) can be used to calculate the density ρ_{N_2}, and therefore the moles of the $N_{2(g)}$ in cylinder 1. Fig. 7 shows the calculated final pressure of $N_{2(g)}$ in cylinder 1 after undergoing expansion at $T = 251.95$ K (−21.2 °C), as a function of the initial pressure of $N_{2(g)}$ in the cylinder at $T = 329.85$ K (56.7 °C), when the apparatus was fueled, reflecting the worst case operating conditions in terms of air temperature extremes for the hydrogen generation apparatus.

It can be noted in Fig. 7 that if the initial $N_{2(g)}$ pressure above $H_2O_{(l)}$ in cylinder 1 is set approximately to 30 atm (441 psi), then the final pressure in the cylinder after all the $H_2O_{(l)}$ has been transferred into cylinder 2 will be 7.72 atm (113 psi) which is sufficiently high to allow a minimum $H_{2(g)}$ gas pressure of 600 kPa (87 psi) to be maintained within cylinder 2. The result in Fig. 7 demonstrates that even under the

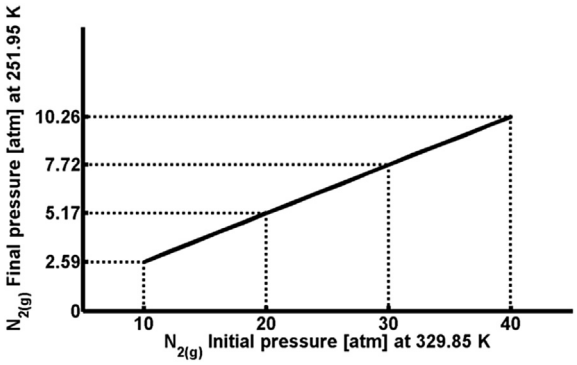

Fig. 7 – Final pressure of $N_{2(g)}$ in cylinder 1 after undergoing expansion to transfer the $H_2O_{(l)}$ from cylinder 1 into cylinder 2.

most extreme air temperature conditions expected to occur within the conterminous 48 states of the U.S.A., it is still possible to operate the hydrogen generation apparatus reliably, without affecting the transfer of the concentrated brine solution reactant derived from seawater and stored in cylinder 1, into cylinder 2, to react with the solid $Na_{(s)}$ metal to generate $H_{2(g)}$ fuel.

The hydrogen generation apparatus shown in Fig. 1, must be capable of generating $H_{2(g)}$ according to Eq. (1) over the full range of expected ambient air temperatures and therefore the chemical reaction has to be spontaneous in the forward direction at temperatures as low as $T = 251.95$ K (−21.2 °C) or as high as $T = 329.85$ K (56.7 °C), corresponding to the eutectic temperature of the aqueous NaCl–H_2O solution and the highest recorded temperature in Death Valley, respectively. Evaluating the likelihood of the chemical reaction to occur in the forward direction requires calculating the Gibbs free energy change of the reaction in Eq. (1) at reference temperature and pressure conditions and also for the stated temperature range of operation from 251.95 K (−21.2 °C) to 329.85 K (56.7 °C). The change in the Gibbs free energy of a chemical reaction at constant temperature is given by Eq. (12) [68].

$$\Delta G = \Delta H - T\Delta S \tag{12}$$

In Eq. (12), ΔG represents the change in the Gibbs free energy, ΔH represents the enthalpy change, and ΔS represents the entropy change of the reaction. Table 6 lists the standard Gibbs free energies of formation ΔG_f°, standard enthalpies of formation ΔH_f° and standard entropies S° of the compounds in Eq. (1) at temperature $T = 298.15$ K and standard atmospheric pressure of $P_0 = 101\,325$ Pa.

Table 6 – Gibbs free energy, enthalpy of formation and entropy at $T = 298.15$ K and $P_0 = 101\,325$ Pa.

	ΔG_f° [kJ/mol]	ΔH_f° [kJ/mol]	S° [J/K·mol]
Sodium ($Na_{(s)}$)	0	0	51.1 ± 0.3 [26]
Pure (VSMOW) Water ($H_2O_{(l)}$)	−237.19 [69]	−285.85 [69]	69.96 [69]
Hydrogen ($H_{2(g)}$)	0	0	130.58 [69]
Sodium Hydroxide ($NaOH_{(s)}$)	−379.651 [50]	−425.8 ± 0.2 [50]	64.43 ± 0.8 [50]

Using the tabulated standard free energies of formation ΔG_f°, in Table 6, it becomes possible to calculate the change in the Gibbs free energy for the H_2 generating chemical reaction in Eq. (1) as shown below in Eq. (13).

$$\Delta G = \left(\Delta G_f^\circ(H_2) + 2\cdot\Delta G_f^\circ(NaOH)\right) - \left(2\cdot\Delta G_f^\circ(Na) + 2\cdot\Delta G_f^\circ(H_2O)\right) = -284.92 \text{ kJ} \tag{13}$$

The result from Eq. (13) of $\Delta G = -284.92$ kJ using pure (VSMOW) water ($H_2O_{(l)}$) is valid at temperature $T = 298.15$ K and pressure $P_0 = 101\,325$ Pa and the large negative value for ΔG shows that under these conditions, the chemical reaction in Eq. (1) will occur spontaneously in the forward direction. The result should also be intuitively familiar because nearly everyone has witnessed that when a small piece of $Na_{(s)}$ metal is placed in a volume of liquid $H_2O_{(l)}$ at room temperature, it immediately reacts to liberate $H_{2(g)}$ gas with the attendant formation of an aqueous $NaOH_{(aq)}$ solution. To calculate if the reaction remains spontaneous in the forward direction over the full temperature range of operation from 251.95 K (−21.2 °C) to 329.85 K (56.7 °C), and not just at $T = 298.15$ K (25 °C), using instead of pure (VSMOW) $H_2O_{(l)}$, seawater concentrated into a brine solution with a Practical Salinity $S_P = 251$ as shown in Fig. 6, yielding the fusion temperature of the seawater $T_{fs} = -21.2$ °C that is equivalent to the eutectic temperature of a 23.18% by weight NaCl in NaCl–H_2O solution shown in Fig. 5, it is necessary to calculate the entropy values of the reactants and products listed in Table 6, as well as the enthalpies of formation of the $H_2O_{(l)}$ and $NaOH_{(s)}$ as a function of temperature. The Eq. (12) can then be used to calculate the resulting change in the Gibbs free energy for the hydrogen generating chemical reaction in Eq. (1) as a function of temperature.

The calculation of the change in entropy as a function of temperature for the reactants and products in Eq. (1), is performed according to Eq. (14).

$$\Delta S^\circ = \int_{T_1}^{T_2} \frac{c_p}{T} dT \tag{14}$$

The calculation of the change in the enthalpies of formation as a function of temperature for $H_2O_{(l)}$ and $NaOH_{(s)}$, is performed according to Eq. (15).

$$\Delta H = \int_{T_1}^{T_2} \Delta c_p dT \tag{15}$$

In Eq. (15), ΔH represents the difference in the enthalpy of formation between the values at T_1 and T_2 while Δc_p represents the difference in the isobaric heat capacities between products and reactants. The Eq. (15) is used to evaluate the chemical reactions provided in Eqs. 16 and 17.

$$H_{2(g)} + \tfrac{1}{2}O_{2(g)} \rightarrow H_2O_{(l)} \tag{16}$$

$$Na_{(s)} + \tfrac{1}{2}O_{2(g)} + \tfrac{1}{2}H_{2(g)} \rightarrow NaOH_{(s)} \tag{17}$$

Calculating the entropy and the enthalpy of formation at different temperatures ranging from 251.95 K (−21.2 °C) to

Table 7 – Heat capacities at constant pressure with $P_0 = 101\,325$ Pa.

	Temperature [K]	c_p [J/K·mol]
Sodium ($Na_{(s)}$)	150–298.15	$33.999 - 7.412 \times 10^{-2}\cdot T - 7.4865 \times 10^{4}\cdot T^{-2} + 2.6801 \times 10^{-4}\cdot T^{2} - 2.536 \times 10^{-7}\cdot T^{3}$ [26]
	298.15–370.95	$53.941 - 194.429 \times 10^{-3}\cdot T + 361.905 \times 10^{-6}\cdot T^{2}$ [26]
Hydrogen ($H_{2(g)}$)	240	28.16 [70]
	250	28.33 [70]
	260	28.48 [70]
	270	28.59 [70]
	280	28.69 [70]
	290	28.78 [70]
	300	28.85 [70]
Sodium Hydroxide ($NaOH_{(s)}$)	250	55.39 [50,71]
	260	56.37 [50,71]
	270	57.30 [50,71]
	280	58.16 [50,71]
	290	58.94 [50,71]
	298.15	59.53 ± 0.3 [50]
	298.15–514	$-797.602 + 5146.32 \times 10^{-3}\cdot T + 87.154 \times 10^{5}\cdot T^{-2} - 11367.7 \times 10^{-6}\cdot T^{2} + 8875.35 \times 10^{-9}\cdot T^{3}$ [50]
Oxygen ($O_{2(g)}$)	250	29.28 [72]
	255	29.29 [72]
	260	29.30 [72]
	265	29.31 [72]
	270	29.32 [72]
	275	29.34 [72]
	280	29.36 [72]
	285	29.37 [72]
	290	29.39 [72]
	295	29.41 [72]
	300	29.44 [72]

329.85 K (56.7 °C), requires knowledge of the isobaric heat capacity c_p, as a function of the temperature which is provided in Table 7 for the sodium (Na), hydrogen (H_2) and sodium hydroxide (NaOH) reactants and products in Eq. (1) and for oxygen (O_2).

The isobaric heat capacity c_p, as a function of the absolute temperature T, absolute pressure P, and absolute salinity S_A, for seawater, can be calculated based on the specific Gibbs energy g, given in Eq. (18) [73].

$$g(S_A, T, P) = g^W(T, P) + g^S(S_A, T, P) \quad \text{J/kg} \tag{18}$$

In Eq. (18), g^W represents the specific Gibbs energy of pure (VSMOW) water ($H_2O_{(l)}$) and g^S represents the specific Gibbs energy of the saline part. The thermodynamic properties of the seawater including the specific isobaric heat capacity c_{ps}, can be calculated by taking the appropriate partial derivatives of the Gibbs function in Eq. (18). The specific isobaric heat capacity c_{ps}, is calculated according to Eq. (19) as the sum of the pure (VSMOW) $H_2O_{(l)}$ and saline specific isobaric heat capacities.

$$c_{ps} = c_{ps}^W + c_{ps}^S = -Tg_{TT}^W - Tg_{TT}^S = -Tg_{TT} \qquad g_{TT} \equiv \left[\frac{\partial^2 g}{\partial T^2}\right] \tag{19}$$

In Eq. (19), T represents the absolute temperature in Kelvin (K) and g_{TT} is defined as the second partial derivative of the specific Gibbs energy g, with respect to the absolute temperature T. The expression for $g_{TT}{}^S$ for calculating the saline part of the specific isobaric heat capacity $c_{ps}{}^S$, is given in Eq. (20) [73].

$$g_{TT}^S(S_A, T, P) = \frac{g^*}{(T^*)^2} \sum_{k=0}^{5} \sum_{j=2}^{6} \sum_{i=2}^{7} j(j-1) g_{ijk} \xi_S^i \tau_S^{j-2} \pi_S^k \quad \text{J/K}^2\cdot\text{kg} \tag{20}$$

The coefficients for calculating Eq. (20) are provided in Table A.2 in Appendix A. In Eq. (20), the reducing specific Gibbs energy $g^* = 1$ J/kg, the reduced temperature is given as $\tau_S = (T - T_0)/T^*$ where the Celsius zero point is given as $T_0 = 273.15$ K, and the reducing temperature $T^* = 40$ K. The reduced pressure is given as $\pi_S = (P - P_0)/P^*$ where the standard atmospheric pressure $P_0 = 101\,325$ Pa, and the reducing pressure $P^* = 1 \times 10^8$ Pa. The reduced salinity is given as $\xi_S = (S_A/S^*)^{0.5}$, and the reducing salinity $S^* = 40.188617$ g/kg.

The specific isobaric heat capacity $c_{ps}{}^W$ of pure (VSMOW) $H_2O_{(l)}$ in Eq. (19), can be calculated based on the specific Helmholtz energy f, for pure (VSMOW) $H_2O_{(l)}$ given in dimensionless form in Eq. (21) [35].

$$\frac{f(\rho_{H_2O}, T)}{R_{H_2O}T} = \phi_{H_2O}(\delta_{H_2O}, \tau_{H_2O}) = \phi^o_{H_2O}(\delta_{H_2O}, \tau_{H_2O}) + \phi^r_{H_2O}(\delta_{H_2O}, \tau_{H_2O}) \tag{21}$$

where,

$$\phi^o_{H_2O} = ln\delta_{H_2O} + n_1^o + n_2^o\tau_{H_2O} + n_3^o ln\tau_{H_2O} + \sum_{i=4}^{8} n_i^o ln\left(1 - e^{-\gamma_i^o \tau_{H_2O}}\right) \tag{22}$$

$$\phi^r_{H_2O} = \sum_{i=1}^{7} n_i \delta_{H_2O}^{d_i} \tau_{H_2O}^{t_i} + \sum_{i=8}^{51} n_i \delta_{H_2O}^{d_i} \tau_{H_2O}^{t_i} e^{-\delta_{H_2O}^{c_i}} + \sum_{i=52}^{54} n_i \delta_{H_2O}^{d_i} \tau_{H_2O}^{t_i} e^{-\alpha_i \left(\delta_{H_2O} - \varepsilon_i\right)^2 - \beta_i \left(\tau_{H_2O} - \gamma_i\right)^2} + \sum_{i=55}^{56} n_i \Delta^{b_i} \delta_{H_2O} \Psi \tag{23}$$

In Eq. (21), $\phi_{H_2O}{}^{o}$ represents an ideal gas part and $\phi_{H_2O}{}^{r}$ represents the residual part of the dimensionless Helmholtz energy ϕ_{H_2O}, with the reduced density and inverse reduced temperature given as $\delta_{H_2O}=\rho_{H_2O}/\rho_{c-H_2O}$ and $\tau_{H_2O}=T_{c-H_2O}/T$, respectively where the critical density $\rho_{c-H_2O}=322\ kg/m^3$, the critical temperature $T_{c-H_2O}=647.096\ K$, and specific gas constant $R_{H_2O}=461.51805\ J/K\cdot kg$. The specific isobaric heat capacity $c_{ps}{}^{W}$ of pure (VSMOW) $H_2O_{(l)}$ is expressed according to Eq. (24) that is based on Eq. (21) [35].

$$\frac{c_{ps}^{W}(\delta_{H_2O},\tau_{H_2O})}{R_{H_2O}}=-\tau_{H_2O}^2\left(\phi^{o}_{\tau\tau_{H_2O}}+\phi^{r}_{\tau\tau_{H_2O}}\right)+\frac{\left(1+\delta_{H_2O}\phi^{r}_{\delta_{H_2O}}+\delta_{H_2O}\tau_{H_2O}\phi^{r}_{\delta\tau_{H_2O}}\right)^2}{1+2\delta_{H_2O}\phi^{r}_{\delta_{H_2O}}+\delta_{H_2O}^2\phi^{r}_{\delta\delta_{H_2O}}} \tag{24}$$

where,

$$\phi^{o}_{\tau\tau_{H_2O}}=-\frac{n_3^{o}}{\tau_{H_2O}^2}-\sum_{i=4}^{8}n_i^{o}\left(\gamma_i^{o}\right)^2e^{-\gamma_i^{o}\tau_{H_2O}}\left(1-e^{-\gamma_i^{o}\tau_{H_2O}}\right)^{-2} \tag{25}$$

$$\begin{aligned}\phi^{r}_{\tau\tau_{H_2O}}=&\sum_{i=1}^{7}n_it_i(t_i-1)\delta_{H_2O}^{d_i}\tau_{H_2O}^{t_i-2}+\sum_{i=8}^{51}n_it_i(t_i-1)\delta_{H_2O}^{d_i}\tau_{H_2O}^{t_i-2}e^{-\delta_{H_2O}^{c_i}}\\&+\sum_{i=52}^{54}n_i\delta_{H_2O}^{d_i}\tau_{H_2O}^{t_i}e^{-\alpha_i\left(\delta_{H_2O}-\varepsilon_i\right)^2-\beta\left(\tau_{H_2O}-\gamma_i\right)^2}\\&\times\left[\left(\frac{t_i}{\tau_{H_2O}}-2\beta_i\left(\tau_{H_2O}-\gamma_i\right)\right)^2-\frac{t_i}{\tau_{H_2O}^2}-2\beta_i\right]\\&+\sum_{i=55}^{56}n_i\delta_{H_2O}\left[\frac{\partial^2\Delta^{b_i}}{\partial\tau_{H_2O}^2}\Psi+2\frac{\partial\Delta^{b_i}}{\partial\tau_{H_2O}}\frac{\partial\Psi}{\partial\tau_{H_2O}}+\Delta^{b_i}\frac{\partial^2\Psi}{\partial\tau_{H_2O}^2}\right]\end{aligned} \tag{26}$$

$$\begin{aligned}\phi^{r}_{\delta_{H_2O}}=&\sum_{i=1}^{7}n_id_i\delta_{H_2O}^{d_i-1}\tau_{H_2O}^{t_i}+\sum_{i=8}^{51}n_ie^{-\delta_{H_2O}^{c_i}}\left[\delta_{H_2O}^{d_i-1}\tau_{H_2O}^{t_i}\left(d_i-c_i\delta_{H_2O}^{c_i}\right)\right]\\&+\sum_{i=52}^{54}n_i\delta_{H_2O}^{d_i}\tau_{H_2O}^{t_i}e^{-\alpha_i\left(\delta_{H_2O}-\varepsilon_i\right)^2-\beta_i\left(\tau_{H_2O}-\gamma_i\right)^2}\left[\frac{d_i}{\delta_{H_2O}}-2\alpha_i\left(\delta_{H_2O}-\varepsilon_i\right)\right]\\&+\sum_{i=55}^{56}n_i\left[\Delta^{b_i}\left(\Psi+\delta_{H_2O}\frac{\partial\Psi}{\partial\delta_{H_2O}}\right)+\frac{\partial\Delta^{b_i}}{\partial\delta_{H_2O}}\delta_{H_2O}\Psi\right]\end{aligned} \tag{27}$$

$$\begin{aligned}\phi^{r}_{\delta\delta_{H_2O}}=&\sum_{i=1}^{7}n_id_i(d_i-1)\delta_{H_2O}^{d_i-2}\tau_{H_2O}^{t_i}+\sum_{i=8}^{51}n_ie^{-\delta_{H_2O}^{c_i}}\\&\times\left[\delta_{H_2O}^{d_i-2}\tau_{H_2O}^{t_i}\left(\left(d_i-c_i\delta_{H_2O}^{c_i}\right)\left(d_i-1-c_i\delta_{H_2O}^{c_i}\right)-c_i^2\delta_{H_2O}^{c_i}\right)\right]\\&+\sum_{i=52}^{54}n_i\tau_{H_2O}^{t_i}e^{-\alpha_i\left(\delta_{H_2O}-\varepsilon_i\right)^2-\beta_i\left(\tau_{H_2O}-\gamma_i\right)^2}\\&\times\left[-2\alpha_i\delta_{H_2O}^{d_i}+4\alpha_i^2\delta_{H_2O}^{d_i}\left(\delta_{H_2O}-\varepsilon_i\right)^2-4d_i\alpha_i\delta_{H_2O}^{d_i-1}\left(\delta_{H_2O}-\varepsilon_i\right)\right.\\&\left.+d_i(d_i-1)\delta_{H_2O}^{d_i-2}\right]+\sum_{i=55}^{56}n_i\left[\Delta^{b_i}\left(2\frac{\partial\Psi}{\partial\delta_{H_2O}}+\delta_{H_2O}\frac{\partial^2\Psi}{\partial\delta_{H_2O}^2}\right)\right.\\&\left.+2\frac{\partial\Delta^{b_i}}{\partial\delta_{H_2O}}\left(\Psi+\delta_{H_2O}\frac{\partial\Psi}{\partial\delta_{H_2O}}\right)+\frac{\partial^2\Delta^{b_i}}{\partial\delta_{H_2O}^2}\delta_{H_2O}\Psi\right]\end{aligned} \tag{28}$$

$$\begin{aligned}\phi^{r}_{\delta\tau_{H_2O}}=&\sum_{i=1}^{7}n_id_it_i\delta_{H_2O}^{d_i-1}\tau_{H_2O}^{t_i-1}+\sum_{i=8}^{51}n_it_i\delta_{H_2O}^{d_i-1}\tau_{H_2O}^{t_i-1}\left(d_i-c_i\delta_{H_2O}^{c_i}\right)e^{-\delta_{H_2O}^{c_i}}\\&+\sum_{i=52}^{54}n_i\delta_{H_2O}^{d_i}\tau_{H_2O}^{t_i}e^{-\alpha_i\left(\delta_{H_2O}-\varepsilon_i\right)^2-\beta_i\left(\tau_{H_2O}-\gamma_i\right)^2}\\&\times\left[\frac{d_i}{\delta_{H_2O}}-2\alpha_i\left(\delta_{H_2O}-\varepsilon_i\right)\right]\left[\frac{t_i}{\tau_{H_2O}}-2\beta_i\left(\tau_{H_2O}-\gamma_i\right)\right]\\&+\sum_{i=55}^{56}n_i\left[\Delta^{b_i}\left(\frac{\partial\Psi}{\partial\tau_{H_2O}}+\delta_{H_2O}\frac{\partial^2\Psi}{\partial\delta_{H_2O}\partial\tau_{H_2O}}\right)+\delta_{H_2O}\frac{\partial\Delta^{b_i}}{\partial\delta_{H_2O}}\frac{\partial\Psi}{\partial\tau_{H_2O}}\right.\\&\left.+\frac{\partial\Delta^{b_i}}{\partial\tau_{H_2O}}\left(\Psi+\delta_{H_2O}\frac{\partial\Psi}{\partial\delta_{H_2O}}\right)+\frac{\partial^2\Delta^{b_i}}{\partial\delta_{H_2O}\partial\tau_{H_2O}}\delta_{H_2O}\Psi\right]\end{aligned} \tag{29}$$

and where,

$$\Delta=\theta^2+B_i\left[\left(\delta_{H_2O}-1\right)^2\right]^{a_i} \tag{30}$$

$$\theta=\left(1-\tau_{H_2O}\right)+A_i\left[\left(\delta_{H_2O}-1\right)^2\right]^{\frac{1}{2\beta_i}} \tag{31}$$

$$\Psi=e^{-C_i\left(\delta_{H_2O}-1\right)^2-D_i\left(\tau_{H_2O}-1\right)^2} \tag{32}$$

$$\frac{\partial\Delta^{b_i}}{\partial\delta_{H_2O}}=b_i\Delta^{b_i-1}\frac{\partial\Delta}{\partial\delta_{H_2O}} \tag{33}$$

$$\frac{\partial^2\Delta^{b_i}}{\partial\delta_{H_2O}^2}=b_i\left\{\Delta^{b_i-1}\frac{\partial^2\Delta}{\partial\delta_{H_2O}^2}+(b_i-1)\Delta^{b_i-2}\left(\frac{\partial\Delta}{\partial\delta_{H_2O}}\right)^2\right\} \tag{34}$$

$$\frac{\partial\Delta^{b_i}}{\partial\tau_{H_2O}}=-2\theta b_i\Delta^{b_i-1} \tag{35}$$

$$\frac{\partial^2\Delta^{b_i}}{\partial\tau_{H_2O}^2}=2b_i\Delta^{b_i-1}+4\theta^2b_i(b_i-1)\Delta^{b_i-2} \tag{36}$$

$$\begin{aligned}\frac{\partial^2\Delta^{b_i}}{\partial\delta_{H_2O}\partial\tau_{H_2O}}=&-A_ib_i\frac{2}{\beta_i}\Delta^{b_i-1}\left(\delta_{H_2O}-1\right)\left[\left(\delta_{H_2O}-1\right)^2\right]^{\frac{1}{2\beta_i}-1}\\&-2\theta b_i(b_i-1)\Delta^{b_i-2}\frac{\partial\Delta}{\partial\delta_{H_2O}}\end{aligned} \tag{37}$$

$$\frac{\partial\Delta}{\partial\delta_{H_2O}}=\left(\delta_{H_2O}-1\right)\left\{A_i\theta\frac{2}{\beta_i}\left[\left(\delta_{H_2O}-1\right)^2\right]^{\frac{1}{2\beta_i}-1}+2B_ia_i\left[\left(\delta_{H_2O}-1\right)^2\right]^{a_i-1}\right\} \tag{38}$$

$$\begin{aligned}\frac{\partial^2\Delta}{\partial\delta_{H_2O}^2}=&\frac{1}{\left(\delta_{H_2O}-1\right)}\frac{\partial\Delta}{\partial\delta_{H_2O}}\\&+\left(\delta_{H_2O}-1\right)^2\left\{4B_ia_i(a_i-1)\left[\left(\delta_{H_2O}-1\right)^2\right]^{a_i-2}\right.\\&+2A_i^2\left(\frac{1}{\beta_i}\right)^2\left\{\left[\left(\delta_{H_2O}-1\right)^2\right]^{\frac{1}{2\beta_i}-1}\right\}^2\\&\left.+A_i\theta\frac{4}{\beta_i}\left(\frac{1}{2\beta_i}-1\right)\left[\left(\delta_{H_2O}-1\right)^2\right]^{\frac{1}{2\beta_i}-2}\right\}\end{aligned} \tag{39}$$

$$\frac{\partial \Psi}{\partial \delta_{H_2O}} = -2C_i\left(\delta_{H_2O} - 1\right)\Psi \tag{40}$$

$$\frac{\partial^2 \Psi}{\partial \delta_{H_2O}^2} = \left\{2C_i\left(\delta_{H_2O} - 1\right)^2 - 1\right\}2C_i\Psi \tag{41}$$

$$\frac{\partial \Psi}{\partial \tau_{H_2O}} = -2D_i\left(\tau_{H_2O} - 1\right)\Psi \tag{42}$$

$$\frac{\partial^2 \Psi}{\partial \tau_{H_2O}^2} = \left\{2D_i\left(\tau_{H_2O} - 1\right)^2 - 1\right\}2D_i\Psi \tag{43}$$

$$\frac{\partial^2 \Psi}{\partial \delta_{H_2O}\partial \tau_{H_2O}} = 4C_iD_i\left(\delta_{H_2O} - 1\right)\left(\tau_{H_2O} - 1\right)\Psi \tag{44}$$

The coefficients provided in Table A.3 in Appendix A are intended for calculating the ideal gas part $\phi_{H_2O}{}^{o}$ and the residual part $\phi_{H_2O}{}^{r}$ of the dimensionless Helmholtz energy ϕ_{H_2O}, for pure (VSMOW) $H_2O_{(l)}$ given in Eqs. 21–24.

Using Eq. (14) in conjunction with the isobaric heat capacities given in Table 7 as well as Eqs. 19–44 in conjunction with corresponding coefficients given in Tables A.2-A.3 in Appendix A, it becomes possible to calculate the entropy values of the reactants and products in Eq. (1) as a function of the temperature ranging from 251.95 K (−21.2 °C) to 329.85 K (56.7 °C). In Fig. 8, the entropies as a function of temperature are calculated for sodium ($Na_{(s)}$), concentrated seawater ($H_2O_{(l)}$) having the Reference Composition with 252.18 g of sea salt solute per kilogram of seawater solution, as well as for hydrogen ($H_{2(g)}$) and sodium hydroxide ($NaOH_{(s)}$).

In Fig. 9, the enthalpies of formation as a function of temperature are calculated for concentrated seawater ($H_2O_{(l)}$) having the Reference Composition with 252.18 g of sea salt solute per kilogram of seawater solution and sodium hydroxide ($NaOH_{(s)}$), respectively. Using the calculated entropies and enthalpies of formation as a function of temperature shown in Figs. 8 and 9, respectively, it becomes possible to calculate the change in the Gibbs free energy of the hydrogen generating chemical reaction in Eq. (1) as a function of the temperature, according to Eq. (12) as shown in Fig. 10.

It is evident from the calculation shown in Fig. 10 that the hydrogen fuel generating chemical reaction of Eq. (1) will occur spontaneously over the required temperature range from 251.95 K (−21.2 °C) to 329.85 K (56.7 °C), since the change in the Gibbs free energy ΔG, remains strongly negative even at the fusion temperature $T_f \approx 251.95$ K of concentrated brine solution. It is therefore expected that hydrogen ($H_{2(g)}$) fuel can be reliably generated according to Eq. (1) over the full temperature range that can prevail in the conterminous 48 states of the U.S.A.

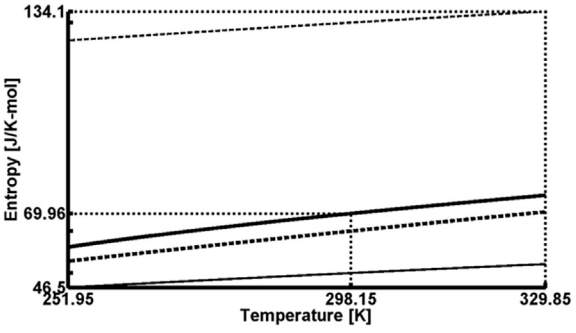

Fig. 8 – Entropy as a function of temperature for sodium ($Na_{(s)}$) (thin solid), seawater ($H_2O_{(l)}$) concentrated to 252.18 g/kg of sea salt (thick solid), hydrogen ($H_{2(g)}$) (thin dash) and sodium hydroxide ($NaOH_{(s)}$) (thick dash).

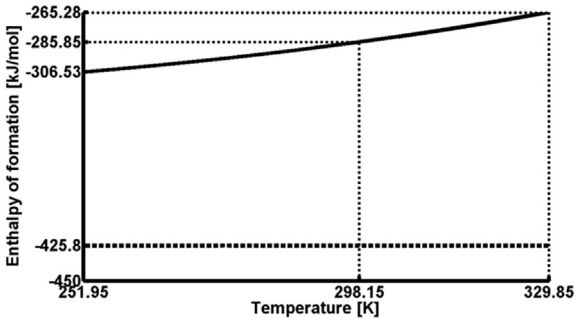

Fig. 9 – Enthalpy of formation as a function of temperature for seawater ($H_2O_{(l)}$) concentrated to 252.18 g/kg of sea salt (solid) and sodium hydroxide ($NaOH_{(s)}$) (dash).

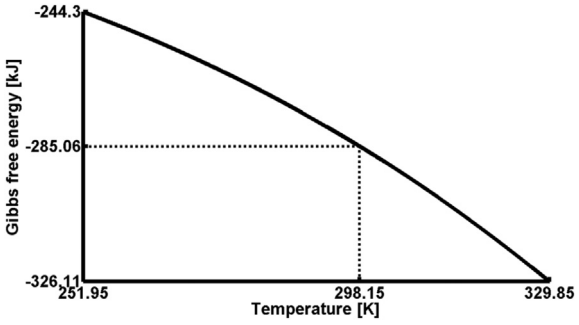

Fig. 10 – Calculated Gibbs free energy ΔG, as a function of temperature for the hydrogen generating reaction in Eq. (1).

The rate at which hydrogen (H_2) gas is produced in cylinder 2 of the hydrogen generation apparatus is an important consideration for motor vehicle propulsion. If a motor vehicle equipped with the 40 cell variant of the hydrogen generation apparatus shown in Fig. 3, has a maximum range of 480 km (298.3 miles) and is capable of achieving a sustained maximum driving speed of 120 km/hr (74.6 mph), then the hydrogen generation apparatus must deliver $H_{2(g)}$ fuel continuously for a duration given as 480 km/120 km/hr = 4 hours or 240 minutes. The $H_{2(g)}$ fuel is produced sequentially in each of the 40 cells of the hydrogen generation apparatus and therefore in each cell the solid $Na_{(s)}$ metal in cylinder 2 must react completely with $H_2O_{(l)}$ transferred from cylinder 1 at a rate given as 240 min/40 cells = 6 min/cell. If the chemical reaction of Eq. (1) occurs at a uniform rate for 6 minutes in each cell to consume all of the Na metal in cylinder 2 and generate H_2 fuel and NaOH byproduct, then the volume quantities of Na metal and NaOH byproduct present in cylinder 2 as a function of time are calculated as shown in Fig. 11.

The temperature of the Na metal and NaOH byproduct in cylinder 2 is calculated as a function of time in Fig. 12 for an

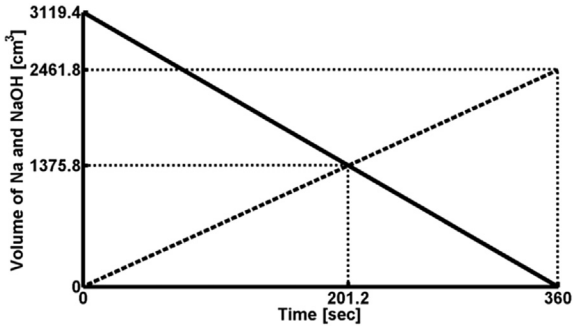

Fig. 11 – Na (solid) and NaOH (dash) volume quantities as a function of time in cylinder 2.

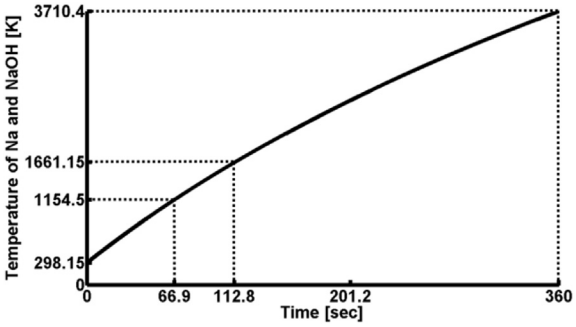

Fig. 12 – Temperature of Na and NaOH as a function of time in cylinder 2.

initial temperature of the Na metal $T_{Na} = 298.15$ K assuming adiabatic heating, due to the exothermic H_2 generating chemical reaction of Eq. (1). Our simulations indicate that when liquid $H_2O_{(l)}$ reactant is introduced into cylinder 2, the rapidly released heat by the exothermic chemical reaction of Eq. (1) is sufficiently high to locally melt the Na metal, and to necessitate cooling of cylinder 2 to prevent a rapid temperature rise as seen in Fig. 12, that can vaporize the Na and NaOH. The NaOH byproduct which is more than twice as dense as Na metal shown in Table 3, will sink or dissolve into the very low viscosity locally melted Na metal and therefore not accumulate as a barrier to the liquid $H_2O_{(l)}$ reacting with the Na metal to generate $H_{2(g)}$ fuel. Even as some NaOH begins to accumulate above the Na metal as the latter is consumed, as seen occurring after time $t = 201.2$ seconds in Fig. 11, the NaOH is generated as particulate matter through which the liquid $H_2O_{(l)}$ can readily percolate to react with the Na metal. Further study is ongoing to ascertain if special geometries of the Na metal might be needed to effect a higher rate of reaction with the liquid $H_2O_{(l)}$, or if alloying the sodium (Na) metal with potassium (K) to lower its melting point might be beneficial to more efficiently absorb or dissolve the denser NaOH byproduct.

Range of a hydrogen generation apparatus equipped vehicle

The novel hydrogen generation apparatus design described in detail in the sections titled Hydrogen generation apparatus characteristics and Hydrogen generation method, has been shown through detailed calculations to be capable of reliably operating under a wide range of ambient temperature conditions that might be encountered in the conterminous 48 states of the U.S.A., and in other regions of the planet where large population concentrations exist. The apparatus design was also meant to be modular, allowing multiple cells to be arrayed to a common fuel line as shown in Fig. 3, to provide the required fuel capacity and range in a motor vehicle. The hydrogen generation system shown in Fig. 3, comprises 40 cells wherein each cell is shown in Fig. 1 to consist of cylinders 1 and 2, for storing $H_2O_{(l)}$ and solid $Na_{(s)}$ metal reactants, respectively. The total quantity of reactants and $H_{2(g)}$ fuel produced is calculated and the result given in Table 8 for the 40 cell hydrogen generation system shown in Fig. 3.

The energy content of the 2622 mol of $H_{2(g)}$ fuel produced by the hydrogen generation apparatus with 40 cells, having the characteristics described in Table 8, is calculated according to the combustion reaction with oxygen (O_2) given in Eq. (45).

$$2622\ H_{2(g)} + 1311\ O_{2(g)} \rightarrow 2622\ H_2O_{(g)} \quad (45)$$

According to the chemical reaction in Eq. (45), the standard enthalpy of formation of one mole of steam ($H_2O_{(g)}$) is given as $\Delta H_f^\circ(H_2O_{(g)}) = -241.84$ kJ/mol [69]. The combustion of 2622 mol of $H_{2(g)}$ fuel produced by the 40 cell hydrogen generator according to Eq. (45), yields a total energy given as $\Delta H = (2622\ \text{mol}) \times (-241.84\ \text{kJ/mol}) = -634\ 104.48$ kJ. To compare the heating value of the $H_{2(g)}$ fuel produced by the 40 cell hydrogen generator with conventional fossil fuel such as 100 octane gasoline, chemically known as 2,2,4-Trimethylpentane (C_8H_{18}), it is necessary to evaluate the respective combustion reaction with O_2 given in Eq. (46).

$$2C_8H_{18(l)} + 25O_{2(g)} \rightarrow 16CO_{2(g)} + 18H_2O_{(g)} \quad (46)$$

According to the chemical reaction in Eq. (46), the standard enthalpies of formation for one mole of 2,2,4-Trimethylpentane, carbon dioxide ($CO_{2(g)}$) and steam ($H_2O_{(g)}$) are given as $\Delta H_f^\circ(C_8H_{18(l)}) = -224.14$ kJ/mol, $\Delta H_f^\circ(CO_{2(g)}) = -393.51$ kJ/mol, and $\Delta H_f^\circ(H_2O_{(g)}) = -241.84$ kJ/mol, respectively [69]. The exothermic reaction of Eq. (46), yields an energy per mole for the combustion of 2,2,4-Trimethylpentane given as $\Delta H_c^\circ = [\{(16\ \text{mol}) \times \Delta H_f^\circ(CO_{2(g)}) + (18\ \text{mol}) \times \Delta H_f^\circ(H_2O_{(g)})\} - (2\ \text{mol}) \times \Delta H_f^\circ(C_8H_{18(l)})]/2 = -5100.5$ kJ/mol. Using the known molar mass of 2,2,4-Trimethylpentane given as 114.22852 g/mol, the energy released per gram of fuel by the combustion

Table 8 – Characteristics of a 40 cell variant of the hydrogen generation apparatus.

	Quantity stored or generated [mol]	Quantity stored or generated [kg]
Sodium (Na)	5244	120.558
[a]Pure (VSMOW) Water (H_2O)	5552	100.020
Hydrogen (H_2)	2622	5.286
Sodium Hydroxide (NaOH)	5244	209.744

[a] Air free water as opposed to air-saturated water, the latter having a freezing point $T = 273.1501$ K [58].

reaction of 2,2,4-Trimethylpentane with O_2 is calculated as (−5100.5 kJ/mol)/(114.229 g/mol) = −44.65 kJ/g [31]. The total mass of 2,2,4-Trimethylpentane fuel that provides the equivalent heating value as the $H_{2(g)}$ fuel produced by the 40 cell hydrogen generator system can be calculated as (−634 104.48 kJ)/(−44.65 kJ/g) = 14 201.67 g. Using the known density of 2,2,4-Trimethylpentane given as 0.6919 g/cm^3, the calculated mass of fuel is converted to a volume as (14 201.67 g)/(0.6919 g/cm^3) = 20 525.61 cm^3 or 20.52561 L (5.4 Gal) [69].

Contemporary motor vehicles are typically equipped with somewhat larger fuel reservoirs of at least 10 Gal in volume due to the need for supplying the unnecessarily large and wasteful, 100+ horse power engines equipping them. By contrast, a volume of 21 L (5.5 Gal) was the standard load of 2,2,4-Trimethylpentane fuel carried by the early generation of the subcompact Fiat 500 series of motor vehicles that utilized a 9.5 kW (12.7 hp) air cooled engine to achieve a driving range in excess of 466 km (289.6 miles) with a top speed of 85 km/hr (52.8 mph). The economical and highly reliable Italian Fiat 500 series of subcompact motor vehicles and their license produced Austrian derivatives such as the Steyr-Daimler-Puch 500, were extremely popular during the 1950s, 60s and 70s in Europe and continue to be prized by enthusiasts and collectors in Europe and the U.S.A. The chassis of such subcompact motor vehicles could be readily manufactured anew and retrofitted with the novel hydrogen generator in place of the normally installed 21 L (5.5 Gal) fuel tank to provide an equal driving range, albeit using cleaner burning $H_{2(g)}$ fuel.

The energy of the hydrogen ($H_{2(g)}$) fuel can be harnessed for useful work more efficiently by conversion in a hydrogen fuel cell to electric power for a motor driving the wheels of the vehicle. To estimate how much more efficient a hydrogen fuel cell equipped electric motor vehicle could be using the hydrogen generation system shown in Fig. 3, comprising 40 hydrogen generating cells, it is necessary first to calculate the energy conversion efficiency of the 9.5 kW (12.7 hp), Model S2 inline 2 cylinder, air cooled internal combustion engine used in the 1957 Fiat 500. An estimate of the energy conversion efficiency of the 9.5 kW (12.7 hp), Model S2 internal combustion engine can be made by assuming that at the maximum driving speed of 85 km/hr, the engine produces 9.5 kW or kJ/sec of power. Engine fuel consumption is given by the manufacturer as 4.5 L per 100 km. The mass of the 21 L (5.5 Gal) standard load of 2,2,4-Trimethylpentane fuel is calculated as (21 000 cm^3)(0.6919 g/cm^3) = 14 529.9 g. The number of moles of 2,2,4-Trimethylpentane fuel is given as (14 529.9 g)/(114.229 g/mol) = 127.2 mol. The combustion of 127.2 mol of 2,2,4-Trimethylpentane fuel according to Eq. (46), yields a total energy given as ΔH = (127.2 mol) × (−5100.5 kJ/mol) = −648 783.6 kJ. The motor vehicle driving range is calculated as (21 L/4.5 L) × (100 km) = 466 km. The driving duration required for the stated driving range of 466 km is then calculated as (466 km/85 km/hr) × 3600 sec/hr = 19 764 sec. The energy conversion efficiency of the Model S2 internal combustion engine is then calculated as [{(9.5 kJ/sec)(19 764 sec)}/648 783.6 kJ] × 100 = 28.9%. The efficiency value of 28.9% is expected for an Otto type internal combustion engine and remains unchanged whether the engine is fueled with fossil fuel or with hydrogen (H_2). By contrast, the energy conversion efficiency of a modern hydrogen fuel cell such as the 75 kW, FCvelocity-HD6 unit manufactured by the Ballard company, ranges between 60 and 70% and requires 99.99% pure $H_{2(g)}$ fuel. Clearly, the use of a modern hydrogen fuel cell in combination with the novel hydrogen generation apparatus described that is capable of producing very high purity $H_{2(g)}$ on demand according to Eq. (1), would provide significant improvement in the energy conversion efficiency of the $H_{2(g)}$ fuel compared with using direct combustion of the $H_{2(g)}$ fuel in an appropriately configured internal combustion engine.

Economic considerations

The hydrogen generation apparatus design presented has been shown to be capable of producing hydrogen ($H_{2(g)}$) fuel on demand according to Eq. (1), under a wide range of ambient temperature conditions from 251.95 K (−21.2 °C) to 329.85 K (56.7 °C) without need for electric heaters, while also delivering a sufficient quantity of the $H_{2(g)}$ fuel given in Table 8, to power a motor vehicle and achieve an equal driving range as with a standard load of gasoline fuel. Fueling the motor vehicle with sodium (Na) metal and seawater to generate environmentally clean H_2 followed by reprocessing of the sodium hydroxide (NaOH) byproduct using electrolysis to recover the Na metal, can also be shown to be safer and more cost competitive than the existing gasoline and diesel fuel counterparts.

The novel hydrogen generation apparatus has been designed to offer greater inherent safety than alternative methods of storing hydrogen such as very high pressure hydrogen gas cylinders that are currently used to provide $H_{2(g)}$ fuel for a small fleet of experimental fuel cell electric vehicles (FCEVs), and to be safer even than the motor vehicles fueled with gasoline. Very high pressure gas cylinders made from composite material used presently to store $H_{2(g)}$ fuel on board FCEVs at pressures as high as 70 MPa (10 153 psi), weigh approximately 70 kg which is significantly less than the 533.9 kg weight of the fully fueled hydrogen generator presented here. Despite lighter weight, the very high pressure gas cylinder made from composite material is inherently dangerous because it is meant to store a full 5 kg load of volatile $H_{2(g)}$ fuel near the occupants of the motor vehicle. A rupture in a 70 MPa (10 153 psi) fully fueled $H_{2(g)}$ tank would likely not afford a chance of escape for the vehicle occupants or even persons nearby. By contrast, the novel hydrogen generator stores nonvolatile solid $Na_{(s)}$ metal in well segregated cylinders so that even if a fire should occur in one of the cylinders, it will take significant time before it can spread to affect the other cells of the hydrogen generation apparatus, thereby providing time for the occupants to escape, or for rescuers to arrive. The nonvolatile solid $Na_{(s)}$ metal has negligible vapor pressure and is therefore safer to store than volatile gasoline which has high vapor pressure under standard atmospheric conditions.

The existing infrastructure of gasoline and diesel fueling stations could be readily upgraded to support dispensing $Na_{(s)}$ metal and seawater while recovering NaOH byproduct with added NaCl in sea salt for later reprocessing by electrolysis

Table 9 – Projected design parameters of the solar tower.

Tower height [m]	Number of levels	PV panels per level	PV panels total	Single PV panel area [m^2]	[a]PV panel efficiency [%]	[b]Solar irradiance [W/m^2]	Total power [MW]
300	100	300	30 000	1	90	887	23.9

[a] PV devices are based on novel, very high transmittance, back-illuminated silicon-on-sapphire wafer substrate [18–21].
[b] AM 1.5D spectrum.

according to Eqs. (2) and (3) at a remote location, to recover the Na metal for reuse in generating $H_{2(g)}$ fuel according to Eq. (1). Gasoline refueling stations store volatile gasoline delivered by tanker truck at night, in 10 000 gallon underground storage tanks (USTs), with most refueling stations having at least two such underground tanks on the premises. To implement the hydrogen fuel, clean energy cycle shown in Fig. 2, at a typical refueling station, the first underground storage tank UST 1, can be used to store seawater for fueling cylinder 1 of the hydrogen generation apparatus while UST 2, can be used to store the recovered sodium hydroxide (NaOH) byproduct with added NaCl in sea salt. Seawater from UST 1 can be pumped into UST 2 to maintain the contents of the latter in a fluid or liquid state. It might be necessary to provide a rubberized coating on the interior of UST 2 to mitigate corrosion effects from the aqueous $NaOH_{(aq)}$. Above ground, a prefabricated building structure can be provided to store the hermetically sealed cylinders shown in Fig. 4, each containing approximately 3 kg of solid $Na_{(s)}$ metal for refueling motor vehicles. A nitrogen (N_2) gas generator would also be needed on the premises for producing dry N_2 gas for pressurizing cylinder 1 of the hydrogen generation apparatus with a properly trained attendant to help refuel the motor vehicles. At night when the refueling station is replenished, the tanker truck delivers seawater to refill UST 1 and hermetically sealed Na metal cylinders shown in Fig. 4, and removes the empty Na metal cylinders and the aqueous $NaOH_{(aq)}$ byproduct with added NaCl in sea salt from UST 2, for reprocessing by electrolysis to recover the Na metal for reuse in generating $H_{2(g)}$ fuel.

The electric power required for electrolysis of recovered NaOH byproduct with added NaCl from seawater can be derived from clean sources such as large hydroelectric power stations or using solar towers, each comprising up to 30 000 spatially arrayed and electrically interconnected PV panels. The electrolysis apparatus can be located inside a factory complex collocated with the solar tower. The electrical cost of electrolysis is estimated from the standard reduction potentials of the oxidation and reduction half reactions that occur at the anode and cathode, respectively of the electrolysis cell when implementing Eqs. (2) and (3) [69].

$$\text{Cathode (reduction):} \quad Na^{+}_{(aq)} + e^{-} \rightarrow Na_{(s)} \qquad E^{\circ}_{r} = -2.71\ \text{V} \tag{47}$$

$$\text{Anode (oxidation):} \quad 2Cl^{-}_{(aq)} \rightarrow Cl_{2(g)} + 2e^{-} \qquad E^{\circ}_{o} = -1.36\ \text{V} \tag{48}$$

$$4OH^{-}_{(aq)} \rightarrow O_{2(g)} + 2H_2O + 4e^{-} \qquad E^{\circ}_{o} = -0.40\ \text{V} \tag{49}$$

From Eqs. (47)–(49), the minimum potentials of $E_{ov}^{\circ} = -4.07$ V and $E_{ov}^{\circ} = -3.11$ V are needed to electrolyze NaCl and NaOH, respectively. These voltages are significantly higher than the potential of $E_{ov}^{\circ} = -1.23$ V needed to electrolyze ordinary $H_2O_{(l)}$ to produce $H_{2(g)}$ at the cathode and $O_{2(g)}$ at the anode, however, the benefit from not having to store volatile $H_{2(g)}$ in very large industrial quantities and to transport it between the production plants and refueling stations, outweighs the added electrical cost of producing the solid $Na_{(s)}$ metal. Table 9 summarizes important projected design parameter values for the solar tower.

If the solar tower with characteristics described in Table 9, operates with a steady total power output of 23.9 MW for 8 hours per day, then using an electrolytic cell voltage $V_{CELL} = 5$ V with a cell current $I_{CELL} \approx 96\,500$ A to effect electrolysis with near 100% efficiency in 50 electrolytic cells containing a mixture of fused $NaOH_{(l)}$ and $NaCl_{(l)}$, will yield approximately 33 000 kg of Na metal per day. If electrolysis is performed on fused or molten sea salt directly, then the resulting metal alloy will have the approximate composition by weight of Na (83.67%), Mg (9.96%), Ca (3.19%), K (3.09%) and Sr (0.06%) based on the mass fractions of the metal ion constituents listed in Table 2, although the Mg and Ca can usually be filtered out from the molten alloy at low temperatures between 100 and 200 °C [8]. Potassium is miscible with Na in all proportions and will remain as a constituent of the alloy while strontium is present in negligible quantity. The presence of potassium in Na is beneficial because it lowers the melting point of the alloy and more importantly, it increases the reactivity with H_2O to generate $H_{2(g)}$ according to Eq. (1) in the hydrogen generation apparatus. Any Mg and Ca impurities that do remain in the resulting Na alloy, will not adversely affect the hydrogen generation apparatus operation because both alkaline earth elements react with H_2O to generate $H_{2(g)}$. The useful production yield can be conservatively estimated at 30 000 kg of packaged Na metal per day which is sufficient to refuel 250 motor vehicles equipped with the 40 cell variant of the hydrogen generation apparatus shown in Fig. 3. If the cost of refueling the hydrogen generation apparatus at the refueling station is set at $10.00 for a 120 kg load of solid $Na_{(s)}$ metal and 100 kg of seawater as shown in Table 8, corresponding to a gasoline equivalent cost of $1.85/gallon based on fuel energy content, then the revenue from refueling 250 motor vehicles per day will be given as (250 refuelings/day)($10.00) = $2500/day. The revenue translates to an annual gross income given as (360 days/yr)($2500/day) = $900,000/year. The level of revenue should be sufficient to employ staff and perform regular maintenance on equipment. To provide sufficient Na metal to refuel all 6 079 057 automobiles registered in 2013 in heavily

populated Los Angeles County once per week, would require the production output from approximately 3500 solar towers with the characteristics described in Table 9. The solar towers would be constructed by the thousands in locations such as the Arizona, New Mexico and Mojave deserts as well as in the wide open expanses of West Texas where the human population is sparse and the weather is mostly warm with high solar illumination all year.

Conclusion

It has been demonstrated through detailed calculation and analysis means, that a novel apparatus and method for generating high purity hydrogen ($H_{2(g)}$) on demand at the time and point of use, can be utilized reliably over a wide range of ambient temperature conditions to supply clean $H_{2(g)}$ fuel either for direct combustion inside internal combustion engines or for fuel cells to generate electricity without contaminating sensitive catalysts that might be present in such fuel cells. Although the energy density of the novel hydrogen generator described is not as high as that of conventional fossil fuels, it is sufficiently high to allow internal combustion engine based motor vehicles to utilize the novel hydrogen generation apparatus safely, while providing a driving range equal to a conventionally fueled internal combustion engine based motor vehicle. Most importantly, the novel method of generating $H_{2(g)}$ fuel enables for the first time a means for completely supplanting nonrenewable fossil fuels with renewable $H_{2(g)}$ fuel that is abundantly available in directly accessible seawater, together with the sodium (Na) in sea salt needed to chemically release the H_2 from seawater. Thus, by using efficient photovoltaic devices of a new type being architected by AG STERN, LLC, to provide the electric energy needed to recycle the sodium (Na) metal by performing electrolysis of the sodium hydroxide (NaOH) byproduct resulting from the $H_{2(g)}$ generating chemical reaction of $Na_{(s)}$ and $H_2O_{(l)}$, it becomes possible to establish a sustainable, closed clean energy cycle that fully obviates the need for nonrenewable hydrocarbon based fossil fuels in motor vehicles.

Appendix A. Tables for the calculation of thermodynamic properties

Table A.1 – Coefficients for calculating the specific Helmholtz energy for nitrogen (N_2) [67].

i	N_i	u_i	v_i	w_i	φ_i	λ_i	σ_i
1	0.924 803 575 275	1.0	0.25	0			
2	−0.492 448 489 428	1.0	0.875	0			
3	0.661 883 336 938	2.0	0.5	0			
4	−1.929 026 492 01	2.0	0.875	0			
5	−0.062 246 930 962 9	3.0	0.375	0			
6	0.349 943 957 581	3.0	0.75	0			
7	0.564 857 472 498	1.0	0.5	1			
8	−1.617 200 0598 7	1.0	0.75	1			
9	−0.481 395 031 883	1.0	2.0	1			
10	0.421 150 636 384	3.0	1.25	1			
11	−0.016 196 223 082 5	3.0	3.5	1			
12	0.172 100 994 165	4.0	1.0	1			
13	0.007 354 489 249 33	6.0	0.5	1			
14	0.016 807 730 547 9	6.0	3.0	1			
15	−0.001 076 266 641 79	7.0	0.0	1			
16	−0.013 731 808 851 3	7.0	2.75	1			
17	0.000 635 466 899 859	8.0	0.75	1			
18	0.003 044 322 794 19	8.0	2.5	1			
19	−0.043 576 233 604 5	1.0	4.0	2			
20	−0.072 317 488 931 6	2.0	6.0	2			
21	0.038 964 431 527 2	3.0	6.0	2			
22	−0.021 220 136 391	4.0	3.0	2			
23	0.004 088 229 815 09	5.0	3.0	2			
24	−0.000 055 199 001 798 4	8.0	6.0	2			
25	−0.046 201 671 647 9	4.0	16.0	3			
26	−0.003 003 117 160 11	5.0	11.0	3			
27	0.036 882 589 120 8	5.0	15.0	3			
28	−0.002 558 568 462 2	8.0	12.0	3			
29	0.008 969 152 645 58	3.0	12.0	4			
30	−0.004 415 133 703 50	5.0	7.0	4			
31	0.001 337 229 248 58	6.0	4.0	4			
32	0.000 264 832 491 957	9.0	16.0	4			
33	19.668 819 401 5	1.0	0.0	2	20	325	1.16
34	−20.911 560 073	1.0	1.0	2	20	325	1.16
35	0.016 778 830 698 9	3.0	2.0	2	15	300	1.13
36	2627.675 662 74	2.0	3.0	2	25	275	1.25

Table A.2 – Coefficients for calculating the saline part of g_{TT} [73].

i	j	k	g_{ijk}
1	0	0	5812.814 566 267 32
2	0	0	1416.276 484 841 97
3	0	0	−2432.146 623 817 94
4	0	0	2025.801 156 036 97
5	0	0	−1091.668 410 429 67
6	0	0	374.601 237 877 840
7	0	0	−48.589 106 902 540 9
1	1	0	851.226 734 946 706
2	1	0	168.072 408 311 545
3	1	0	−493.407 510 141 682
4	1	0	543.835 333 000 098
5	1	0	−196.028 306 689 776
6	1	0	36.757 162 299 580 5
2	2	0	880.031 352 997 204
3	2	0	−43.066 467 597 804 2
4	2	0	−68.557 250 920 449 1
2	3	0	−225.267 649 263 401
3	3	0	−10.022 737 086 187 5
4	3	0	49.366 769 485 625 4
2	4	0	91.426 044 775 125 9
3	4	0	0.875 600 661 808 945
4	4	0	−17.139 757 741 978 8
2	5	0	−21.660 324 087 531 1
4	5	0	2.496 970 095 695 08
2	6	0	2.130 169 708 471 83
2	0	1	−3310.491 540 448 39
3	0	1	199.459 603 073 901
4	0	1	−54.791 913 353 288 7
5	0	1	36.028 419 561 108 6
2	1	1	729.116 529 735 046
3	1	1	−175.292 041 186 547
4	1	1	−22.668 355 851 282 9
2	2	1	−860.764 303 783 977
3	2	1	383.058 066 002 476
2	3	1	694.244 814 133 268
3	3	1	−460.319 931 801 257
2	4	1	−297.728 741 987 187
3	4	1	234.565 187 611 355
2	0	2	384.794 152 978 599
3	0	2	−52.294 090 928 133 5
4	0	2	−4.081 939 789 122 61
2	1	2	−343.956 902 961 561
3	1	2	83.192 392 780 181 9
2	2	2	337.409 530 269 367
3	2	2	−54.191 726 251 711 2
2	3	2	−204.889 641 964 903
2	4	2	74.726 141 138 756
2	0	3	−96.532 432 010 745 8
3	0	3	68.044 494 272 645 9
4	0	3	−30.175 511 197 116 1
2	1	3	124.687 671 116 248
3	1	3	−29.483 064 349 429
2	2	3	−178.314 556 207 638
3	2	3	25.639 848 738 991 4
2	3	3	113.561 697 840 594
2	4	3	−36.487 291 900 158 8
2	0	4	15.840 817 276 682 4
3	0	4	−3.412 519 324 412 82
2	1	4	−31.656 964 386 073
2	2	4	44.204 035 830 8
2	3	4	−11.128 273 432 641 3
2	0	5	−2.624 801 565 909 92
2	1	5	7.046 588 033 154 49
2	2	5	−7.920 015 472 116 82

Table A.3 – Coefficients for calculating the specific Helmholtz energy for pure (VSMOW) water ($H_2O_{(l)}$) [35].

i	c_i	d_i	t_i	n_i	n_i^o	γ_i^o		
1	–	1	−0.5	0.012 533 547 935 523	−8.320 446 483 749 7	–		
2	–	1	0.875	7.895 763 472 282 8	6.683 210 527 593 2	–		
3	–	1	1	−8.780 320 330 356 1	3.006 32	–		
4	–	2	0.5	0.318 025 093 454 18	0.012 436	1.287 289 67		
5	–	2	0.75	−0.261 455 338 593 58	0.973 15	3.537 342 22		
6	–	3	0.375	−0.007 819 975 168 798 1	1.279 50	7.740 737 08		
7	–	4	1	0.008 808 949 310 213 4	0.969 56	9.244 377 96		
8	1	1	4	−0.668 565 723 079 65	0.248 73	27.507 510 5		
9	1	1	6	0.204 338 109 509 65				
10	1	1	12	−0.000 066 212 605 039 687				
11	1	2	1	−0.192 327 211 560 02				
12	1	2	5	−0.257 090 430 034 38				
13	1	3	4	0.160 748 684 862 51				
14	1	4	2	−0.040 092 828 925 807				
15	1	4	13	0.393 434 226 032 54 E-6				
16	1	5	9	−0.759 413 770 881 44 E-5				
17	1	7	3	0.000 562 509 793 518 88				
18	1	9	4	−0.156 086 522 571 35 E-4				
19	1	10	11	0.115 379 964 229 51 E-8				
20	1	11	4	0.365 821 651 442 04 E-6				
21	1	13	13	−0.132 511 800 746 68 E-11				
22	1	15	1	−0.626 395 869 124 54 E-9				
23	2	1	7	−0.107 936 009 089 32				
24	2	2	1	0.017 611 491 008 752				
25	2	2	9	0.221 322 951 675 46				
26	2	2	10	−0.402 476 697 635 28				
27	2	3	10	0.580 833 999 857 59				
28	2	4	3	0.004 996 914 699 080 6				
29	2	4	7	−0.031 358 700 712 549				
30	2	4	10	−0.743 159 297 103 41				
31	2	5	10	0.478 073 299 154 8				
32	2	6	6	0.020 527 940 895 948				
33	2	6	10	−0.136 364 351 103 43				
34	2	7	10	0.014 180 634 400 617				
35	2	9	1	0.008 332 650 488 071 3				
36	2	9	2	−0.029 052 336 009 585				
37	2	9	3	0.038 615 085 574 206				
38	2	9	4	−0.020 393 486 513 704				
39	2	9	8	−0.001 655 405 006 373 4				
40	2	10	6	0.001 995 557 197 954 1				
41	2	10	9	0.000 158 703 083 241 57				
42	2	12	8	−0.163 885 683 425 3 E-4				
43	3	3	16	0.043 613 615 723 811				
44	3	4	22	0.034 994 005 463 765				
45	3	4	23	−0.076 788 197 844 621				
46	3	5	23	0.022 446 277 332 006				
47	4	14	10	−0.626 897 104 146 85 E-4				
48	6	3	50	−0.557 111 185 656 45 E-9				
49	6	6	44	−0.199 057 183 544 08				
50	6	6	46	0.317 774 973 307 38				
51	6	6	50	−0.118 411 824 259 81				
i	c_i	d_i	t_i	n_i	α_i	β_i	γ_i	ε_i
52	–	3	0	−31.306 260 323 435	20	150	1.21	1
53	–	3	1	31.546 140 237 781	20	150	1.21	1
54	–	3	4	−2521.315 434 169 5	20	250	1.25	1
i	a_i	b_i	B_i	n_i	C_i	D_i	A_i	β_i
55	3.5	0.85	0.2	−0.148 746 408 567 24	28	700	0.32	0.3
56	3.5	0.95	0.2	0.318 061 108 784 44	32	800	0.32	0.3

REFERENCES

[1] Schüth F, Bogdanovic B, Felderhoff M. Light metal hydrides and complex hydrides for hydrogen storage. Chem Commun 2004;20:2249–58.
[2] Zaluski L, Zaluska A, Strom-Olsen JO. Hydrogenation properties of complex alkali metal hydrides fabricated by mechano-chemical synthesis. J Alloys Compd 1999;290(1–2):71–8.
[3] Bogdanovic B, Schwickardi M. Ti-doped alkali metal aluminum hydrides as potential novel reversible hydrogen storage materials. J Alloys Compd 1997;253–254:1–9.
[4] Zhang Y, Liao S, Xu Y. Highly active alkali metal hydrides; their catalytic syntheses and properties. J Mol Catal 1993;84(3):211–21.
[5] Brown HC. Boranes in organic chemistry. Ithaca, New York: Cornell University Press; 1972. p. 39–49, 209–26.
[6] Millero FJ, Feistel R, Wright DG, McDougall TJ. The composition of standard seawater and the definition of the reference-composition salinity scale. Deep-Sea Res Part I Oceanogr Res Pap 2008;55(1):50–72.
[7] Guernsey EW, Sherman MS. The mechanism of the fixation of nitrogen as sodium cyanide. J Am Chem Soc 1925;47(7):1932–40.
[8] Sittig M. Sodium its manufacture, properties and uses. New York: Reinhold Publishing Corporation; 1956. p. 47–89, 129–42. 242.
[9] Sakintuna B, Lamari-Darkrim F, Hirscher M. Metal hydride for solid hydrogen storage: a review. Int J Hydrogen Energy 2007;32(9):1121–40.
[10] De Jongh PE, Allendorf M, Vajo JJ, Zlotea C. Nanoconfined light metal hydrides for reversible hydrogen storage. MRS Bull 2013;38(6):488–94.
[11] Klebanoff LE, Keller JO. 5 Years of hydrogen storage research in the U.S. DOE metal hydride center of excellence (MHCoE). Int J Hydrogen Energy 2013;38(11):4533–76.
[12] Hagström MT, Lund PD, Vanhanen JP. Metal hydride storage for near-ambient temperature and atmospheric pressure applications, a PDSC study. Int J Hydrogen Energy 1995;20(11):897–909.
[13] Knowlton RE. An investigation of the safety aspects in the use of hydrogen as a ground transportation fuel. Int J Hydrogen Energy 1984;9(1–2):129–36.
[14] Hord J. Is hydrogen a safe fuel? Int J Hydrogen Energy 1978;3(2):157–76.
[15] Davy H. The Bakerian lecture: on some new phenomena of chemical changes produced by electricity, particularly the decomposition of the fixed alkalies, and the exhibition of the new substances which constitute their bases; and on the general nature of alkaline bodies. Philos Trans R Soc Lond 1808;98:1–44.
[16] Castner HY. Process of manufacturing sodium and potassium. U.S. Patent 452,030; 1891.
[17] Downs JC. Electrolytic process and cell. U.S. Patent 1,501,756; 1924.
[18] Stern AG. Design of high quantum efficiency and high resolution, Si/SiGe avalanche photodiode focal plane arrays using novel, back-illuminated, silicon-on-sapphire substrates. In: Park JW, editor. Photodiodes – world activities in 2011. Vienna: InTech publisher; 2011. p. 267–312. ISBN: 978-953-307-530-3.
[19] Stern AG. Design of a high sensitivity emitter-detector avalanche photodiode imager using very high transmittance, back-illuminated, silicon-on-sapphire. SPIE J Opt Eng 2012;51(6):063206.
[20] Stern AG. Very high transmittance, back-illuminated, silicon-on-sapphire semiconductor wafer substrate for high quantum efficiency and high resolution, solid-state, imaging focal plane arrays. U.S. Patent 8,354,282; 2013.
[21] Stern AG. Thin, very high transmittance, back-illuminated, silicon-on-sapphire semiconductor substrates bonded to fused silica. U.S. Patent 8,471,350; 2013.
[22] Chen KF, Kao CM, Chen CW, Surampalli RY, Lee MS. Control of petroleum-hydrocarbon contaminated groundwater by intrinsic and enhanced bioremediation. J Environ Sci 2010;22(6):864–71.
[23] Konecny F, Bohacek Z, Müller P, Kovarova M, Sedlackova I. Contamination of soils and groundwater by petroleum hydrocarbons and volatile organic compounds – case study: ELSLAV BRNO. Bull Geosci 2003;78(3):225–39.
[24] Wilson SC, Jones KC. Bioremediation of soil contaminated with polynuclear aromatic hydrocarbon (PAHs): a review. Environ Pollut 1993;81(3):229–49.
[25] Oriel JA, Lubbock I, Goodliffe AH. Improved apparatus for reacting sodium and water. British Patent 574,360; 1946.
[26] Alcock CB, Chase MW, Itkin VP. Thermodynamic properties of the group IA elements. J Phys Chem Ref Data 1994;23(3):385–497.
[27] Chiong YS. Viscosity of liquid sodium and potassium. In: Proceedings of the Royal Society. Series A, mathematical and physical sciences 1936;157:264–77.
[28] Battezzati AL, Greer AL. The viscosity of liquid metals and alloys. Acta Metall 1989;37(7):1791–802.
[29] Savage HW, Cobb WG. High-temperature centrifugal pumps. Chem Eng Prog 1954;50(9):445–8.
[30] Brill EF. Development of special pumps for liquid metals. Mech Eng 1953;75(5):369–73.
[31] Wieser ME. Atomic weights of the elements 2005 (IUPAC technical report). Pure Appl Chem 2006;78(11):2051–66.
[32] Lewis EL, Perkin RG. Salinity: its definition and calculation. J Geophys Res 1978;83(C1):466–78.
[33] Lewis EL. The practical salinity scale 1978 and its antecedents. IEEE J Ocean Eng 1980;5(1):3–8.
[34] Riser SC, Ren L, Wong A. Salinity in ARGO. Oceanography 2008;21(1):56–67.
[35] Wagner W, Pruß A. The IAPWS formulation 1995 for the thermodynamic properties of ordinary water substance for general and scientific use. J Phys Chem Ref Data 2002;31(2):387–535.
[36] Gonfiantini R. Standards for stable isotope measurements in natural compounds. Nature 1978;271(5645):534–6.
[37] Audi G, Wapstra AH, Thibault C. The AME2003 atomic mass evaluation: (II). Tables, graphs and references. Nucl Phys A 2003;729(1):337–676.
[38] Hagen EB. Ueber die Wärmeausdehnung des Natriums, des Kaliums und deren Legirung im festen und im geschmolzenen Zustande. Annalen der Physik 1883;255(7):436–74.
[39] Tanaka M, Girard G, Davis R, Peuto A, Bignell N. Recommended table for the density of water between 0 °C and 40 °C based on recent experimental reports. Metrologia 2001;38(4):301–9.
[40] Sharqawy MH, Lienhard JH, Zubair M. Thermophysical properties of seawater: a review of existing correlations and data. Desalin Water Treat 2010;16(1–3):354–80.
[41] Lemmon EW, Huber ML, Leachman JW. Revised standardized equation for hydrogen gas densities for fuel consumption applications. J Res Natl Inst Stand Technol 2008;113(6):341–50.
[42] Eberz A. Elektrolytische Leitfähigkeit und Dichte des Systems Wasser Natriumhydroxid im gesamten Mischungsbereich bis maximal 450 Grad C und 3000 bar. 1987. Karlsruhe.

[43] Pickering SU. The hydrates of sodium, potassium, and lithium hydroxides. J Chem Soc Trans 1893;63:890–909.
[44] Cohen-Adad R, Tranquard A, Péronne R, Negri P, Rollet AP. Le système eau-hydroxyde de sodium. Compte rendus de l'académie des sciences 1960;251:2035–7.
[45] Rollet AP, Cohen-Adad R. Les systems "eau-hydroxyde alcalin". Revue de Chimie minérale 1964;1:451–78.
[46] Woldman NE, Gibbons RC. Engineering alloys. 5th ed. New York: Van Nostrand Reinhold Company; 1973. p. 1374–424.
[47] Feistel R, Wagner W. High-pressure thermodynamic Gibbs function of ice and sea ice. J Mar Res 2005;63(1):95–139.
[48] Feistel R, Wagner W. A new equation of state for H_2O ice lh. J Phys Chem Ref Data 2006;35(2):1021–47.
[49] Goodwin RD. Melting pressure equation for the hydrogens. Cryogenics 1962;2(6):353–5.
[50] Gurvich LV, Bergman GA, Gorokhov LN, Iorish VS, Leonidov VYa, Yungman VS. Thermodynamic properties of alkali metal hydroxides. Part 1. Lithium and sodium hydroxides. J Phys Chem Ref Data 1996;25(4):1211–76.
[51] Glasgow AR, Murphy ET, Willingham CB, Rossini FD. Purification, purity, and freezing points of 31 hydrocarbons of the API-NBS series. J Res Natl Bureau Stand 1946;37(2):141–5.
[52] Finke HL, Gross ME, Waddington G, Huffman HM. Low-temperature thermal data for the nine Normal paraffin hydrocarbon from octane to hexadecane. J Am Chem Soc 1954;76(2):333–41.
[53] Makansi MM, Muendel CH, Selke WA. Determination of the vapor pressure of sodium. J Phys Chem 1955;59(1):40–2.
[54] Grilly ER. The vapor pressures of hydrogen, deuterium and tritium up to three atmospheres. J Am Chem Soc 1951;73(2):843–6.
[55] Wartenberg HV, Albrecht P. Vapor pressure of some salts. Zeitschrift für Elektrochemie 1921;27:162–7.
[56] Wiener H. Structural determination of paraffin boiling points. J Am Chem Soc 1947;69(1):17–20.
[57] Egloff G, Sherman J, Dull RB. Boiling Point relationships among aliphatic hydrocarbons. J Phys Chem 1940;44(6):730–45.
[58] Doherty BT, Kester DR. Freezing-point of seawater. J Mar Res 1974;32(2):285–300.
[59] Budretsky AB. Information bulletin of Soviet Antarctic expedition. No. 105. Leningrad: Hydrometeoizdat; 1984.
[60] Wilson GH. The hottest region in the United States. Mon Weather Rev 1915;43(6):278–80.
[61] Court A. How hot is death valley? Geogr Rev 1949:214–20.
[62] Preston-Thomas H. The international temperature scale of 1990 (ITS-90). Metrologia 1990;27(1):3–10.
[63] Bodnar RJ. Revised equation and table for determining the freezing point depression of H_2O-NaCl solutions. Geochim Cosmochim Acta 1993;57(3):683–4.
[64] Hall DL, Sterner SM, Bodnar RJ. Freezing point depression of NaCl-KCl-H_2O solutions. Econ Geol 1988;83(1):197–202.
[65] Daly D, Halbleib M, Smith JI, Gibson WP, Doggett MK, Taylor GH, et al. Physiographically sensitive mapping of climatological temperature and precipitation across the conterminous United States. Int J Climatol 2008;28(15):2031–64.
[66] Millero FJ, Leung WH. The thermodynamics of seawater at one atmosphere. Am J Sci 1976;276(9):1035–77.
[67] Span R, Lemmon EW, Jacobsen RT, Wagner W, Yokozeki A. A reference equation of state for the thermodynamic properties of nitrogen for temperatures from 63.151 to 1000 K and pressures to 2200 MPa. J Phys Chem Ref Data 2000;29(6):1361–433.
[68] Gibbs JW. On the equilibrium of heterogeneous substances. Am J Sci 1878;16(96):441–58.
[69] Weast RC. Handbook of chemistry and physics. Cleveland, Ohio: CRC Press; 1976–1977. C415, D67-D78, D79-D84, D141-D146.
[70] Hilsenrath J, Beckett CW, Benedict WS, Fano L, Hoge HJ, Masi JF, et al. Tables of thermal properties of gases. US Department of Commerce, National Bureau of Standards Circular 564; 1955. p. 267–96.
[71] Murch LE, Giauque WF. The thermodynamic properties of sodium hydroxide and its monohydrate. Heat capacities to low temperatures. Heats of solution. J Phys Chem 1962;66(10):2052–9.
[72] Stewart RB, Jacobsen RT, Wagner W. Thermodynamic properties of oxygen from the triple point to 300 K with pressures to 80 MPa. J Phys Chem Ref Data 1991;20(5):917–1021.
[73] Feistel R. A Gibbs function for seawater thermodynamics for −6 to 80 °C and salinity up to 120 g kg^{-1}. Deep-Sea Res I 2008;55(12):1639–71.